

132861

FINAL REPORT

DEVELOPMENT OF A (Hg,Cd)Te PHOTODIODE DETECTOR  
PHASE II

Contract Period  
19 May 1970 through August 1972

Contract No. NAS5-21197

Placed By  
National Aeronautics & Space Administration  
Goddard Space Flight Center  
Greenbelt, Maryland

(NASA-CR-132861) DEVELOPMENT OF A (Hg, Cd)Te PHOTODIODE DETECTOR, PHASE 2 Final Report, 19 May 1970 - Aug. 1972 (Honeywell, Inc.) 64 p HC \$5.25	N74-10434  Unclas CSCL 14B G3/14 21948
---	---



HONEYWELL  
Radiation Center  
2 Forbes Road  
Lexington, Massachusetts 02173

FINAL REPORT

DEVELOPMENT OF A (Hg,Cd)Te PHOTODIODE DETECTOR  
PHASE II

Contract Period  
19 May 1970 through August 1972

Contract No. NAS5-21197

Placed By  
National Aeronautics & Space Administration  
Goddard Space Flight Center  
Greenbelt, Maryland

Approved By: J. J. Schlickman  
J. J. Schlickman  
Manager  
Product Research  
and Engineering

R. M. Russell  
R. M. Russell  
Program Manager

HONEYWELL  
Radiation Center  
2 Forbes Road  
Lexington, Massachusetts 02173

# TABLE OF CONTENTS

SECTION	TITLE	PAGE
	PREFACE . . . . .	iii
	ABSTRACT . . . . .	iv
	INTRODUCTION AND SUMMARY . . . . .	1
1	THEORY . . . . .	3
1.1	EFFICIENCY . . . . .	3
1.2	FREQUENCY RESPONSE . . . . .	5
1.3	PHOTODIODE NOISE SOURCES AND THE EFFECT OF AMPLIFIER NOISE . . . . .	8
1.4	THEORETICAL LIMITS ON PERFORMANCE . . . . .	11
1.4.1	Detectivity . . . . .	11
1.4.2	Quantum Efficiency--Bandwidth Product or $\eta \cdot f^*$ . . . . .	13
1.5	JUNCTION PROPERTIES . . . . .	15
1.6	JUNCTION FORMATION . . . . .	17
1.7	FREQUENCY MEASUREMENTS . . . . .	17
2	(Hg,Cd)Te PHOTOVOLTAIC DETECTOR . . . . .	21
2.1	JUNCTION FORMATION . . . . .	21
2.2	DIODE FABRICATION . . . . .	21
2.3	JUNCTION PROPERTIES FOR Hg DIFFUSED DIODES . . . . .	24
2.3.1	Temperature Dependence of Reverse Saturation Characteristic . . . . .	24
2.3.2	Comparison of Saturation Current with Theoretical Estimate . . . . .	27
2.3.3	Frequency Response Measurement . . . . .	28
3	CONCLUSIONS AND RECOMMENDATIONS . . . . .	34
	GLOSSARY . . . . .	35
APPENDIX		
A	TEST RESULTS ON 10.6 MICRON (Hg,Cd)Te PHOTODIODES . . . . .	38
A.1	ION IMPLANTED PV-(Hg,Cd)Te ARRAY . . . . .	38
APPENDIX		
B	TEST REPORTS FOR DELIVERED UNITS . . . . .	43

## PREFACE

This report, submitted March 1973, describes work performed under contract NAS5-21197 during the period from May 1970 through August 1972. The program has been conducted at the Honeywell Radiation Center, Lexington, Massachusetts. The NASA program monitors have been J. McElroy and S. Cohen at the Goddard Space Flight Center. A number of scientists and technicians have contributed to the program. D. A. Soderman and A. B. Timberlake were the principal investigators. R. Lancaster and H. I. Andrews supported this program through the (Hg,Cd)Te material growth and characterization. V. Mazurczyk and T. Koehler assisted in the preparation of the final report. D. Maloney fabricated the devices.

## ABSTRACT

High speed sensitive (Hg,Cd)Te photodiode detectors operating in the 77 to 90 °K temperature range have been developed for the 10.6  $\mu\text{m}$  spectral region. P-N junctions formed by impurity (gold) diffusion in p-type (Hg,Cd)Te have been investigated. These photodiodes of approximately  $3 \times 10^{-3} \text{ cm}^2$  area have exhibited responsivities between 20 and 360 V/W, external quantum efficiencies between 2 and 50%, specific detectivities  $D^*_\lambda$  (11.5, 1 kHz, 1 Hz) between  $0.7$  and  $1.7 \times 10^{10} \text{ cm Hz}^{1/2}/\text{W}$ , and response times between 7 and 1.5 ns. The 1.5 ns is not a diode limitation but is believed to be caused by a high inductance of the package. It is shown that the bandwidth and quantum efficiency of a diode are a constant for a fixed ratio of mobility/lifetime ratio of minority carriers. The minority carrier mobility and lifetime uniquely determine the bandwidth and quantum efficiency and indicate the shallow n on p (Hg,Cd)Te diodes are preferable as high performance, high frequency devices.

## INTRODUCTION AND SUMMARY

Advanced high data rate, intersatellite communications systems envisioned and under construction by NASA/Goddard Space Flight Center will require highly sophisticated infrared detectors. In order to utilize the capabilities of the CO<sub>2</sub> laser fully, a photodetector sensitive to 10.6- $\mu$ m radiation with an electrical bandwidth in the GHz range must be developed. Furthermore, for the detector to be useful in spacecraft systems, it should not require cooling below liquid nitrogen temperature.

Although there are 10.6- $\mu$ m photodetectors with properties which approach some of the electrical bandwidth, quantum efficiency, and temperature requirements, there are none which meet all of these. Thus, Honeywell has been engaged in a program with NASA/Goddard to develop a mercury cadmium telluride photodiode with a 3-dB roll-off frequency greater than 800 MHz, a quantum efficiency design goal, Honeywell has directed its efforts first towards producing photodiodes with consistent, reproducible characteristics and then towards optimizing those characteristics to meet the goals of this effort.

The material properties of the alloy semiconductor mercury cadmium telluride (Hg,Cd)Te are ideally suited to this application because of the following characteristics: (1) a continuously variable energy gap, permitting the peak responsivity to be tuned to 10.6  $\mu$ m; (2) an intrinsic photodetector, allowing high performance operation in the 77 to 100 °K temperature range; (3) a coefficient and resulting in a very high quantum efficiency; (4) a high electron mobility, yielding very short transit times and a large electrical bandwidth; and (5) a well-established material growth and detector fabrication technology, yielding high performance (Hg,Cd)Te photoconductive detectors for the 8-14  $\mu$ m spectral region.

During the first phase of this contract, Honeywell has made substantial progress in the investigation of (Hg,Cd)Te material properties and diffusion techniques required for the fabrication of high speed (Hg,Cd)Te photodiodes. Temperature dependent Hall coefficient and resistivity measurements have been made to select classical n and p-type (Hg,Cd)Te. P-N junctions have been formed by impurity (gold) diffusion in n-type material and by stoichiometric deviation (mercury) diffusion in p-type material. Radioactive tracer and electrical measurements on the diffused surface layer have suggested a two-step diffusion mechanism in (Hg,Cd)Te material.

One gold diffused photodiode at 77 °K with an 11.5  $\mu\text{m}$  peak spectral response and  $4 \times 10^{-3} \text{ cm}^2$  area exhibited responsivity between 100 and 360 V/W, external quantum efficiency between 16 and 50%, specific detectivity between 0.7 and  $1.7 \times 10^{10} \text{ cm Hz}^{1/2}/\text{W}$ , and 40-nanosecond response time with 0.9  $\mu\text{m}$  radiation. These performance characteristics vary with dc reverse bias; however, they do not change as the detector operating temperature is increased to 90 °K. The response time is limited by electrical circuit constraints through the product of the junction capacitance and series resistance of the particular contact configuration on the diffused layer which has not been optimized for high speed operation.

The reverse bias currents in the fabricated photodiodes are larger than expected at low temperatures; thus, several experiments to investigate surface inversion and bulk diffusion material properties have been initiated. Voltage dependent junction capacitance and resistance measurements have been made to further the understanding of the junction characteristics.

The performance of photodiodes fabricated by mercury in-diffusion (stoichiometric deviation) has not been as extensively analyzed as the gold diffused photodiodes, however the zero bias responsivity and detectivity measurements made on a number of photodiodes with peak spectral responses in the 8.6 to 11.5- $\mu\text{m}$  range are encouraging. The zero bias performance characteristics of several mercury diffused photodiodes at 77 °K have shown responsivities between 20 and 200 V/W, external quantum efficiencies between 2 and 24%, and specific detectivities as high as  $1.5 \times 10^{10} \text{ cm Hz}^{1/2}/\text{W}$ . Response time measurements were made using pulsed 0.9- $\mu\text{m}$  radiation ranging from 20 to 50 nanoseconds and CO<sub>2</sub> laser (10.6- $\mu\text{m}$  radiation) heterodyne detection ranging from 16 nanoseconds to less than 7 nanoseconds. The heterodyne laser equipment limited this frequency response measurement to 25 MHz.

# SECTION 1

## THEORY

### 1.1 EFFICIENCY

The efficiency for a photodiode operating in the short circuit current mode has been solved exactly for the geometry of Figure 1 by M. B. Prince. The case which he considered is somewhat different from the application to be discussed here. In particular we shall consider the case of infinite d.

In the spirit of the article by Prince

$$\eta = \eta_n + \eta_p$$

$$\eta_n = \alpha L_p \frac{-e}{\alpha L_p + 1} - \frac{[\exp(1 - \alpha L_p) \frac{X_j}{L_p} - \alpha L_p + S [\exp(1 - \alpha L_p) \frac{X_j}{L_p}] - 1]}{(\alpha^2 L_p^2 - 1) (\cosh \frac{X_j}{L_p} + S \sinh \frac{X_j}{L_p})} \quad (1)$$

$$\eta_p = \alpha L_n \frac{e^{-\alpha X_j}}{\alpha L_n + 1} = \frac{e^{-\alpha X_j}}{1 + \frac{1}{\alpha L_n}} \quad (2)$$

This calculation assumes an abrupt junction whose width is small in comparison with  $1/\alpha$  or  $L$ . When this is not the case the carriers absorbed in the depletion region need to be taken into account. The net result is that fewer carriers are absorbed in the p and n regions so that the efficiency will increase.

Equations 1 and 2 take on simple forms for three cases:

- |                                |                          |                  |
|--------------------------------|--------------------------|------------------|
| 1. Shallow Junction            | $X_j \sim 0$             |                  |
| 2. Intermediate depth Junction | $e^{-\alpha X_j} > 0$    | $\alpha L_p > 1$ |
| 3. Deep Junction               | $e^{-\alpha X_j} \sim 0$ | $\alpha L_n > 1$ |



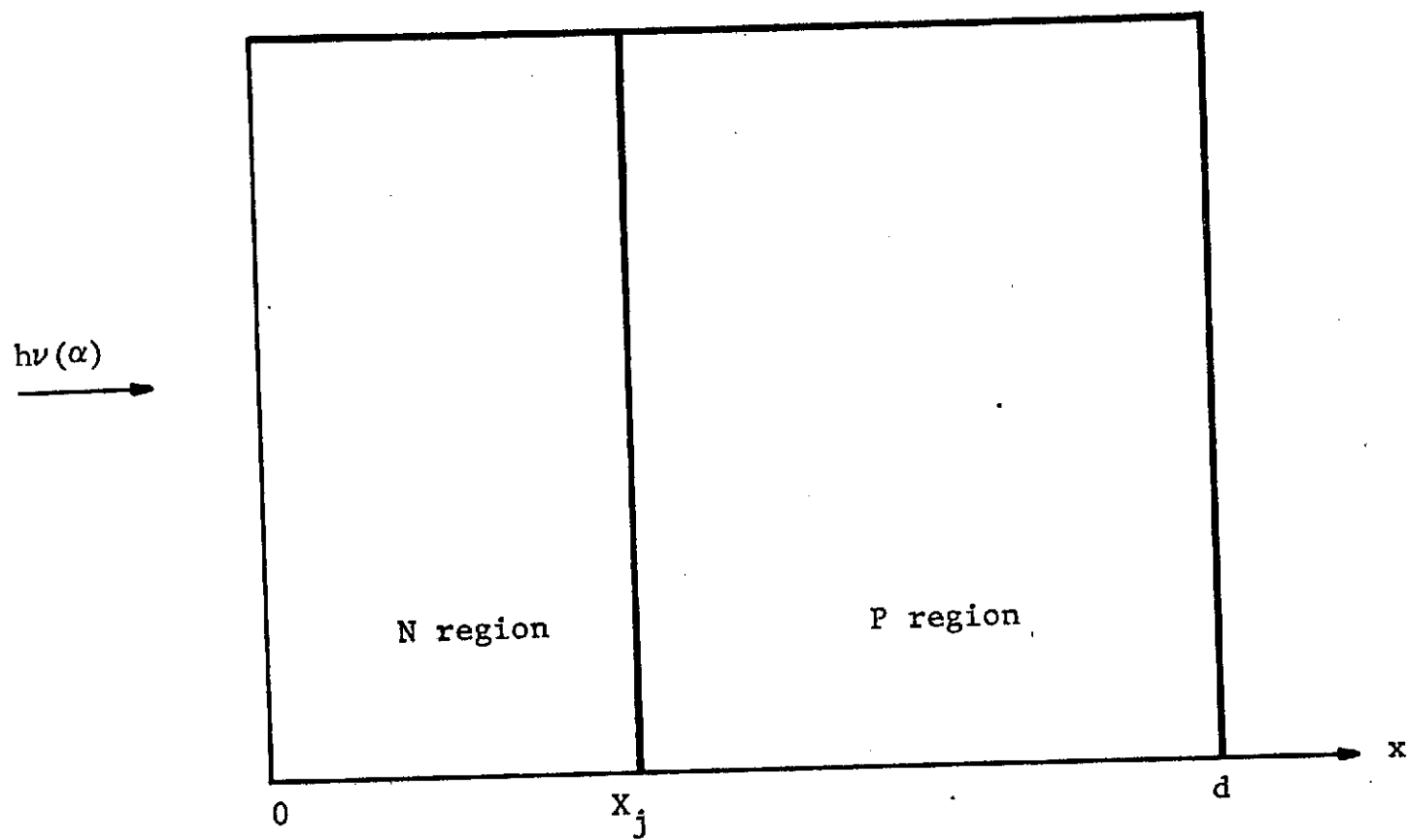


Figure 1 (Hg,Cd)Te DIODE GEOMETRY

For shallow junctions,  $X_j \sim 0$  the maximum efficiency is given by

$$\eta_n \sim \frac{1-r}{1+\frac{1}{\alpha L_n}} \sim 1-r \text{ for } \alpha L_n > 1 \quad (3)$$

Intermediate case

$$\eta_n \sim \frac{(1-S/\alpha L_p)(1-r)}{(1-\frac{1}{\alpha^2 L_p^2})(\cosh \frac{X_j}{L_p} + S \sinh \frac{X_j}{L_p})} \sim \frac{1-r}{\cosh \frac{X_j}{L_p} + S \sinh \frac{X_j}{L_p}} \quad (4)$$

$$\eta_p \sim \frac{e^{-\alpha X_j}}{1+1/\alpha L_n} (1-r) \quad (5)$$

For deep junctions,  $e^{-\alpha X_j} \sim 0$ ,  $X_j \gg 1/\alpha$

$$\eta = \eta_n \sim \frac{1-r}{\cosh \frac{X_j}{L_p} + S \sinh \frac{X_j}{L_p}} \quad (6)$$

In this case the best efficiency occurs for  $S = 0$  and small  $X_j/L_p$  which implies  $L_p \gg X_j$ . For p on n structures the same equations result with p and n interchanged.

## 1.2 FREQUENCY RESPONSE

The frequency response due to carriers generated in the n layer (or p) has been considered.<sup>2,3</sup> The cut-off frequency for the case of  $S = 0$  is

$$W = \frac{2.4 D_p}{X_j^2} \quad (7)$$

$D_p$  is the diffusion coefficient and for M-B statistics

$$D_p = \frac{kT}{q} \mu_p \quad (8)$$

Carriers generated in the depletion region have a very high cut-off frequency because the carriers are swept across the junction by the built-in field. The time constant for this process is approximately

$$\gamma = \frac{X_j}{V_{\text{drift}}} \quad (9)$$

$V_{\text{drift}}$  has been measured as a function of field for several semiconductors as its value approaches  $10^7$  cm/s

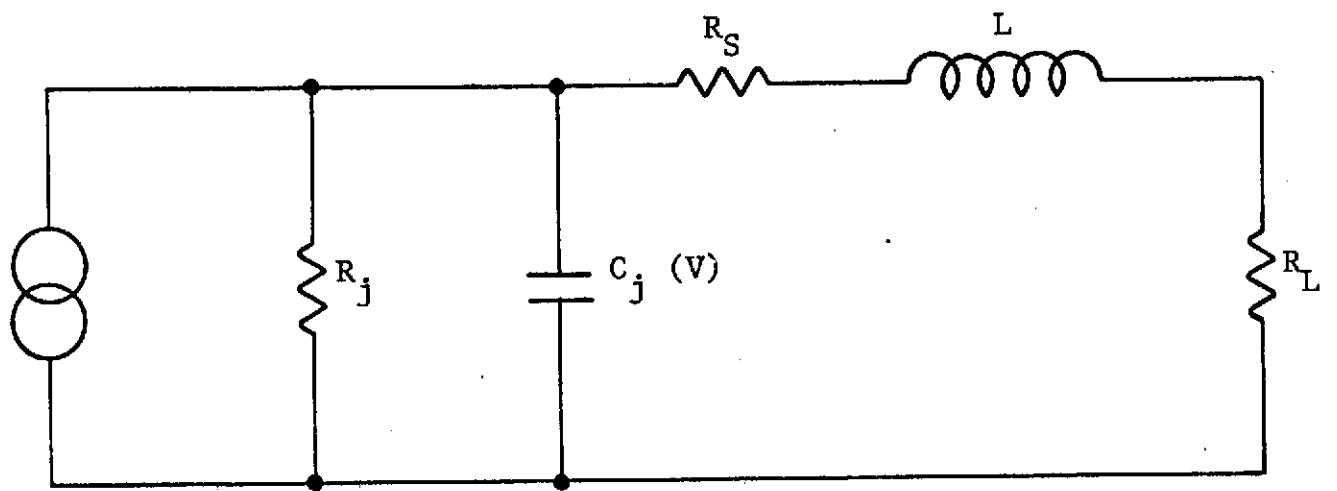
Carriers generated in the p region have a cut-off frequency similar to those in the n region. It is given by

$$\gamma = \frac{\tau_e}{(1 + \alpha_{L_n})}, \quad f_e = \frac{1}{2\pi \tau_e} (1 + \alpha_{L_n}) \quad (10)$$

Assuming no other limiting factors the photocurrent as a function of frequency will show a plateau structure as each contribution rolls off. The magnitude of each roll off will be determined by the number of carriers absorbed in each region.

Beside the frequency roll off due to material parameters one also needs to consider the limitations of the circuit. Figure 2. shows an equivalent circuit for the detector amplifier combination. For frequencies less than 50 MHz the problem of junction capacitance in limiting frequency response is circumvented by using an operational amplifier in the current mode. In this case the amplifier impedance is very small ( $R_L = R_F/A$ ) so that the  $C_j R_L$  product is very small. The current gain is just  $R_F$ .

For frequencies on the order of GHz this option is not available. To achieve the necessary speed a voltage mode amplifier with bandwidth, low gain, and low input impedance is used. The price paid for using such an amplifier is that detectivity delivered by the diode is greatly reduced by the shunting effect of the low input impedance.



$$\frac{1}{R_j} = \frac{e^{-qV/kT}}{R_o} + \frac{1}{R_{Sh}}$$

Figure 2 SIGNAL EQUIVALENT CIRCUIT

Since the diode is to be mounted in a dewar its effect must also be considered. Electrical contact must be made to the diode without appreciably increasing the capacitance and inductance of the circuit. If this condition is met then the limiting circuit parameter will just be  $R_L C_j$ . The voltage across the input is proportional to the term

$$|Z| = R_L \left\{ \left( 1 + \frac{R_L + R_S}{R_L} - W^2 L C_j \right)^2 + W^2 \left[ C_j (R_L + R_S) + \frac{L}{R_j} \right]^2 \right\}^{-1/2} \quad (11)$$

which predicts rapid roll off of signal with frequency. The capacitance of the diode also needs to be kept small to prevent roll off at frequencies

$$W \sim \frac{1}{(R_L + R_S) C_j} \quad (12)$$

### 1.3 PHOTODIODE NOISE SOURCES AND THE EFFECT OF AMPLIFIER NOISE

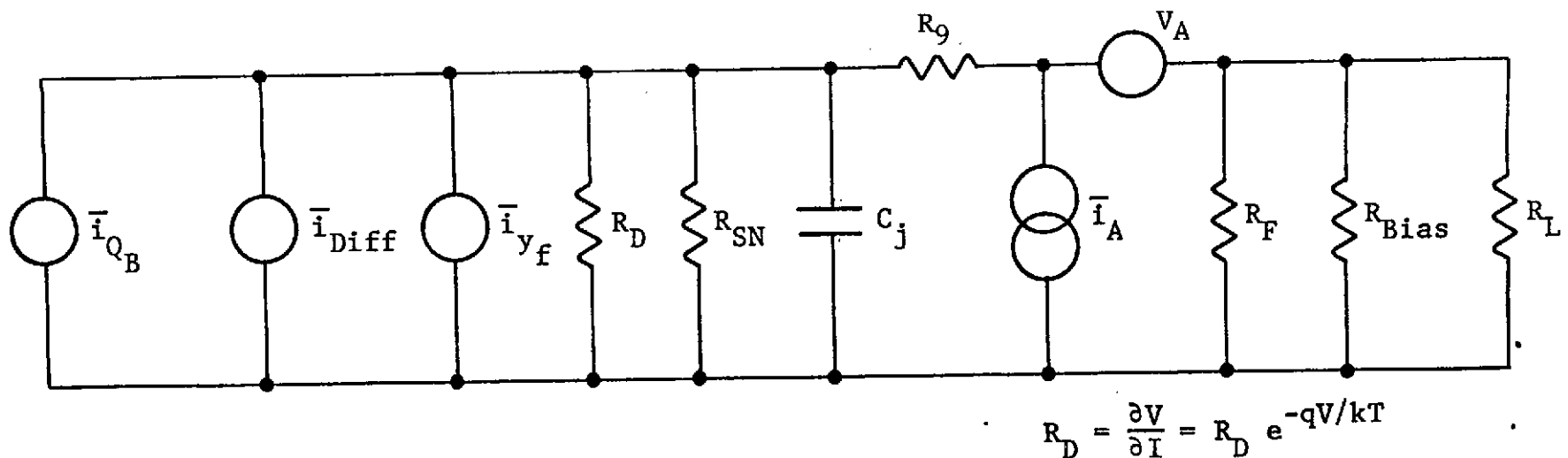
Although the Avantek amplifier (discussed in Section 2.3) operates in the voltage mode i.e., it amplifies the voltage which appears across the input resistor  $R_L$ , the value of  $R_L$  will be less than the diode impedance except for the most severely shunted diodes. Under these conditions and assuming that the stray inductance is small enough such that  $WL < R_L + R_S$  the total noise will be given by

$$i_t^2 = \left[ i_{sn}^2 + i_D^2 + i_{1/f}^2 + i_B^2 \right]_{\text{Detector}} + \left[ i_a^2 + i^2(V_a) \right]_{\text{Amplifier}}$$

The various terms in the noise expression are summarized in the noise equivalent circuit in Figure 3. The various terms are:

$$1) \quad i_D^2 = \frac{2 k T}{R_D} (e^{qV/kT} + 1)$$

which combines the thermal noise and shot noise associated with the diffusion current.



### NOISE SOURCES

1. Short circuit shot noise from background  $\overline{i}^2 = 2\eta q^2 A(Q_S + Q_B)$
2. Shot noise and thermal noise from  $R_D$   $\overline{i}_D^2 = \frac{2kT}{R_0} (e^{qV/kT} + 1)$
3. Thermal noise of Shunt  $R_{sh}$   $i_{sh}^2 = \frac{4kT}{R_{sh}}$
4. 1/f noise  $\overline{i}_{1/f}^2 = \frac{1}{f} [k_1(\frac{V^2}{R_{sh}}) + k_2(I - \frac{V}{sh})^2 + k_3 I^2]$
5. Thermal noise of series resistance  $i_s^2 = 4kTR_s / (R_s + \frac{R_{sh}R_D}{R_{sh} + R_D})^2$
6. Amplifier noise  $i_{na}^2$

Figure 3 NOISE EQUIVALENT CIRCUIT

$$2) \quad i_B^2 = 2 \eta q^2 A Q_B$$

which is the shot noise due to the total background induced current .

$$3) \quad i_{1/f}^2 = \frac{k_1}{f} \frac{V^2}{R_{sh}}$$

1/f noise due to the shunt leakage.

- 4) Thermal noise sources exist of the various resistances in the circuit such as the bias circuit series load, series resistance, shunt resistance, amplifier input termination and feedback resistor in the case of operational amplifiers. This noise would be expressed as a sum of terms in the form

$$i_T^2 = \sum_j \frac{4 k T_j}{R_j}$$

The amplifier is represented by equivalent noise voltage and current sources. Their contribution to the current noise is

$$i_a^2 + v_a^2 \left[ \left( \frac{R_S + R_J}{R_S R_J} \right)^2 + w^2 C_j^2 \right]$$

For the Avantek amplifier used

$$\begin{aligned} v_a &\sim 10^{-9} \text{ v}/\sqrt{\text{Hz}} \\ i_a &\sim 10^{-11} \text{ A}/\sqrt{\text{Hz}} \end{aligned}$$

In the heterodyne operation mode all these noise terms can become insignificant in comparison to the photon induced noise due to the local oscillator:

$$\bar{i}_{LD}^2 = 2 \eta q^2 A Q_{LD}$$

## 1.4 THEORETICAL LIMITS ON PERFORMANCE

With the results on quantum efficiency and noise sources, we can define the ultimate limits of performance for a photodiode in terms of the minority carrier properties of mobility and lifetime.

### 1.4.1 Detectivity

The spectral detectivity ( $D^*_\lambda$ ) per unit bandwidth is defined as:

$$D^*_\lambda = \frac{S_\lambda}{NEI} \sqrt{A_D} \quad (13)$$

where  $S_\lambda$  is the current responsivity in amps/watt,  $A_D$  is the area in  $\text{cm}^2$ , and  $NEI$  is the noise equivalent current of the diode. The maximum detectivity possible occurs when the diode is limited by the thermal noise of the junction resistance. Thus, the minimum

$$NEI = \left[ \frac{2 k T}{R_j} (e^{qV/kT} + 1) \right]^{1/2} \quad (14)$$

when  $V > -.5$  volts.

$$NEI = \sqrt{\frac{2 k T}{R_j}} \quad (15)$$

$$S_\lambda = \frac{\eta \lambda q}{hc} \quad (\text{Amp.Watt}) \quad (16)$$

Therefore,

$$D^*_\lambda = \frac{\eta \lambda q \sqrt{RA}}{hc \sqrt{2 k T}} \quad (17)$$

Figure 4 is a plot of  $D^*_\lambda$  for an 11- $\mu\text{m}$  diode at 80 °K as a function of  $\eta$  and RA product with a 300 °K background. This figure shows that a device with a 20% quantum efficiency needs RA greater than 0.67 ohm- $\text{cm}^2$  to be background limited. RA is uniquely determined by the saturation current density  $J_S$  (equation 14)

$$RA = \frac{kT}{q J_S} \quad (18)$$



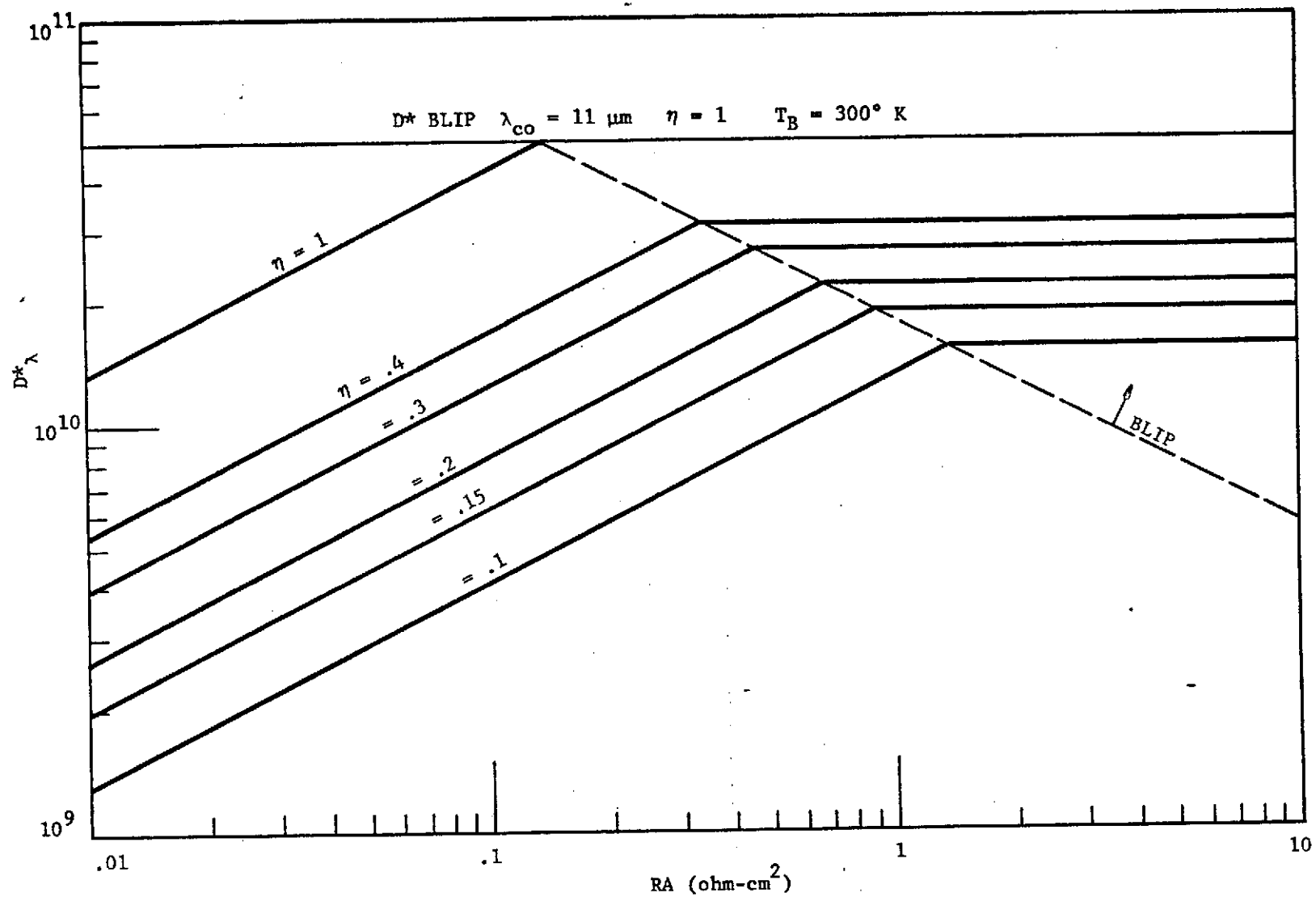


Figure 4

which, in turn, depends on the material parameters of doping and minority carrier mobility and lifetime.

#### 1.4.2 Quantum Efficiency--Bandwidth Product or $\eta^*f^*$

For heterodyne operation, knowing the detectivity is not sufficient to define performance. It is useful to think of the quantum efficiency/cutoff frequency product as a figure of merit for heterodyne operation similar to the  $D^*f^*$  product. No generality is lost because  $D^*$  can easily be recovered via Figure 4.

The assumption is made that the junction is shallow and the depletion width is small in comparison to the diffusion length in the bulk.

The quantum efficiency, or "eta-star", is given by equation 3

$$\eta^* = \frac{1 - r}{1 + \frac{1}{\alpha L_D}} \quad (19)$$

The diffusion length ( $L_D$ ) is valid for either electrons or holes depending on what type of material the substrate is.

The bandwidth of  $f^*$  is defined by equation 10:

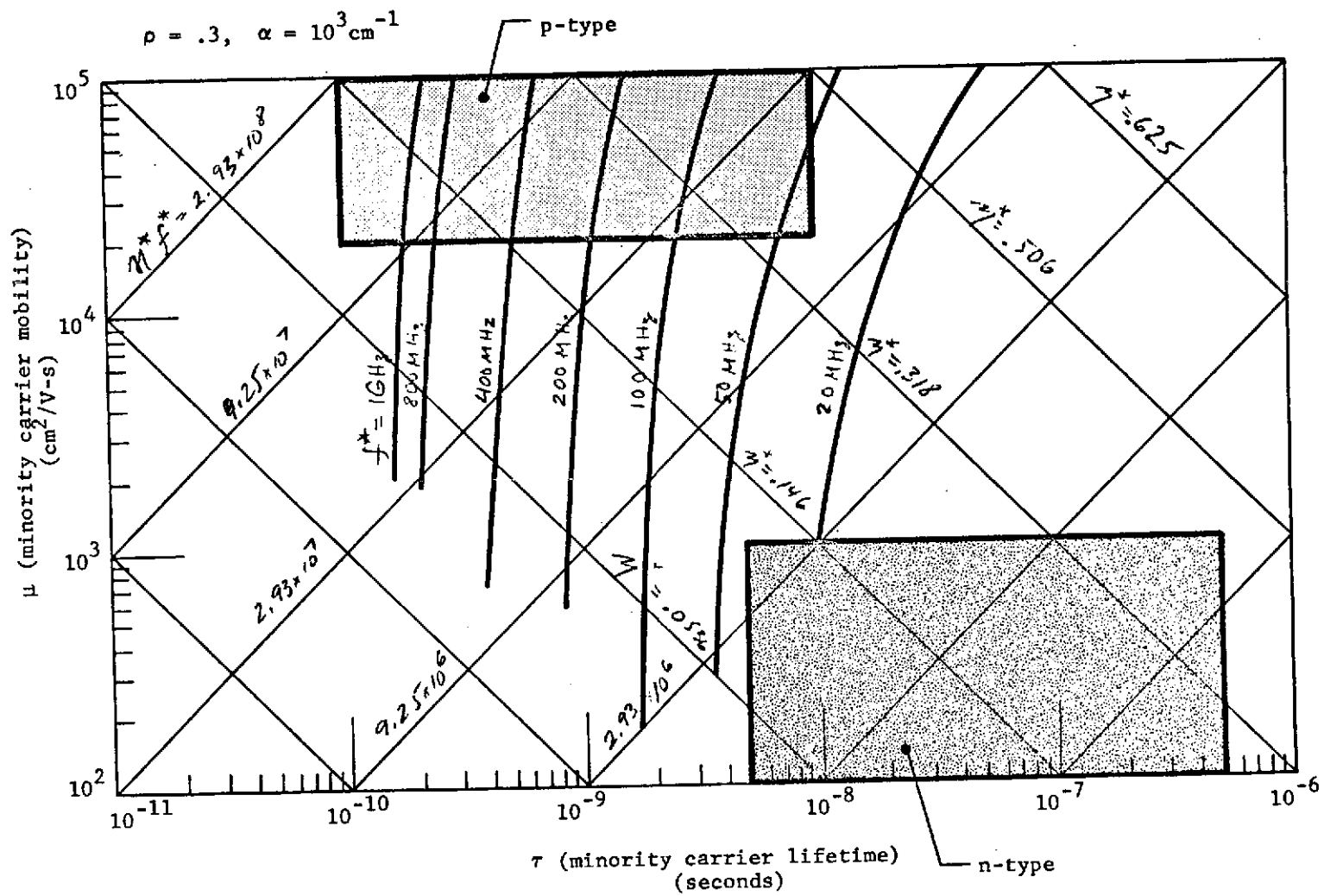
$$f^* = \frac{1}{2\pi\tau} (1 + \alpha L_D) \quad (20)$$

Therefore,

$$\eta^*f^* = \frac{(1 - r)\alpha}{2\pi} \frac{kT}{q} \frac{\mu}{\tau} \quad (21)$$

These three equations allow the construction of a log-log graph as shown in Figure 5 which relates the performance parameters to the material minority carrier properties. Lines of constant thermal velocity of  $\mu/\tau$  define  $\eta^*f^*$ ; lines of constant diffusion length or  $\mu\tau$  define  $\eta^*$ .

We do not know the precise minority carrier properties of (Hg,Cd)Te, but we can define broad existence regions for p-type and n-type, as shown in Figure 5.



m Figure 5  $\eta^* f^*$  (ABRUPT SHALLOW JUNCTION)

The conclusions that can be drawn from Figure 5 are the following:

1. Shallow n-on-p diodes will never exceed 30 MHz.
2. Shallow p-on-n junctions can achieve  $f^*$  greater than 1 GHz, but must trade off quantum efficiency for this. Therefore, a 800 MHz, 20% quantum efficiency device is feasible.
3. To maximize  $\eta^*f^*$ , a material must have maximum mobility and minimum lifetime. This implies a small effective mass for the minority carrier band. (Hg,Cd)Te p-type meets these requirements.
4. Data of 50% quantum efficiency and 1 GHz bandwidth should be viewed with skepticism. This sort of measurement reflects the procedure where efficiency is measured at low frequencies and the contribution from the slow n-layer enhances the quantum efficiency. An exception to this may be P-I-N structures.

#### 1.5 JUNCTION PROPERTIES

The reverse current voltage characteristic for an ideal diode is given by

$$J = J_S (e^{-qV/kT} - 1) \quad (22)$$

$$J_S = q n_i^2 \left[ \frac{L_p}{N_D \tau_p} + \frac{L_n}{N_A \tau_n} \right] + \frac{q n_i W}{\tau_r} \quad (23)$$

$W$  = junction width  
 $J_S$  = recombination time within the junction  
 $n_i$  = intrinsic carrier concentration  
 $L_p$  = minority carrier diffusion length in n region  
 $L_p = \sqrt{D_p \tau_p}$ ;  $D_p = \sqrt{kT/q \mu_p}$  for M-B statistics  
 $L_n$  = minority carrier diffusion length in p region  
 $N_D$  = donor concentration in n region  
 $N_A$  = acceptor concentration in p region  
 $\tau_p$  = minority carrier lifetime in n region  
 $\tau_n$  = minority carrier lifetime in p region

The corresponding junction width and capacitance is given for abrupt junctions by

$$C = \sqrt{\frac{q K \epsilon_o N_B}{2(V_{Bi} \pm V)}} \text{ farad/cm}^2 - \text{abrupt junction} \quad (24)$$

$$W = \frac{K \epsilon_o}{C} = \sqrt{\frac{w(V_{Bi} \pm V) K \epsilon_o}{q N_B}}, \quad N_B = \frac{N_A N_D}{N_A + N_A} \quad (25)$$

and for linearly graded junctions by

$$C = \left( \frac{q a (K \epsilon_o)^2}{12(V_{Bi} \pm V)} \right)^{1/3} \quad (26)$$

$$W = \left[ \frac{K \epsilon_o 12(V_{Bi} \pm V)}{q a} \right]^{1/3}; \text{ charge gradient} = \frac{q a}{K \epsilon_o} \quad (27)$$

A third type of structure in the PIN diode which consists of an intrinsic layer sandwiched between an n and p layer. The width of the junction is independent of the material properties and the capacitance is given by

$$C = \frac{K \epsilon_o}{W} \quad (28)$$

For high speed applications this is the most desirable structure because the front surface layer can be made very thin ( $<1/\alpha$ ) and W very large. The result is that all the carriers are absorbed in the W region giving maximum quantum efficiency at the highest speed. In addition the capacitance of the diode is very small, because W is large, resulting in a small RC circuit parameter. However, this type of structure is very difficult to achieve unless the various layers can be grown consecutively by vapor or liquid phase epitaxy and the doping of each layer controlled.

## 1.6 JUNCTION FORMATION

Junction formation by impurity diffusion has proved to be a highly reliable and controllable process. The diffusion coefficient in a limited temperature range can be described by

$$D(T) = D_0 \exp (-\Delta E/kT)$$

where  $D_0$  is the diffusion coefficient extrapolated to infinite temperature and  $E$  is the activation energy of diffusion.

The simple one dimensional diffusion process can be given by the Fick equation

$$\frac{\partial C(x, t)}{\partial t} = D \frac{\partial^2 C(x, t)}{\partial x^2} \quad (29)$$

where  $C$  is the impurity concentration and  $D$  the diffusion coefficient. For a limited source condition with the total amount of impurities  $S$ , the solution of Equation 29 is given by the Gaussian function

$$C(x, t) = \frac{S}{\sqrt{\pi Dt}} \exp\left(-\frac{x^2}{4Dt}\right) \quad (30)$$

For the constant surface concentration condition, with a surface concentration  $C_s$ , the solution of Equation 29 is given by the error function complement

$$C(x, t) = C_s \operatorname{erfc} \left( \frac{x}{2 \sqrt{Dt}} \right) \quad (31)$$

In practice diffusion profiles can be approximated by either abrupt or linearly graded junctions.

## 1.7 FREQUENCY MEASUREMENTS

Frequency response measurements were made using a klystron modulated  $\text{CO}_2$  laser heterodyne system developed by Dr. V. Corcoran at Martin Marietta, Orlando, Florida. A diagram of the system is shown in Figure 6. Sum and difference signal frequencies are generated by mixing in a waveguide loaded with GaAs the output

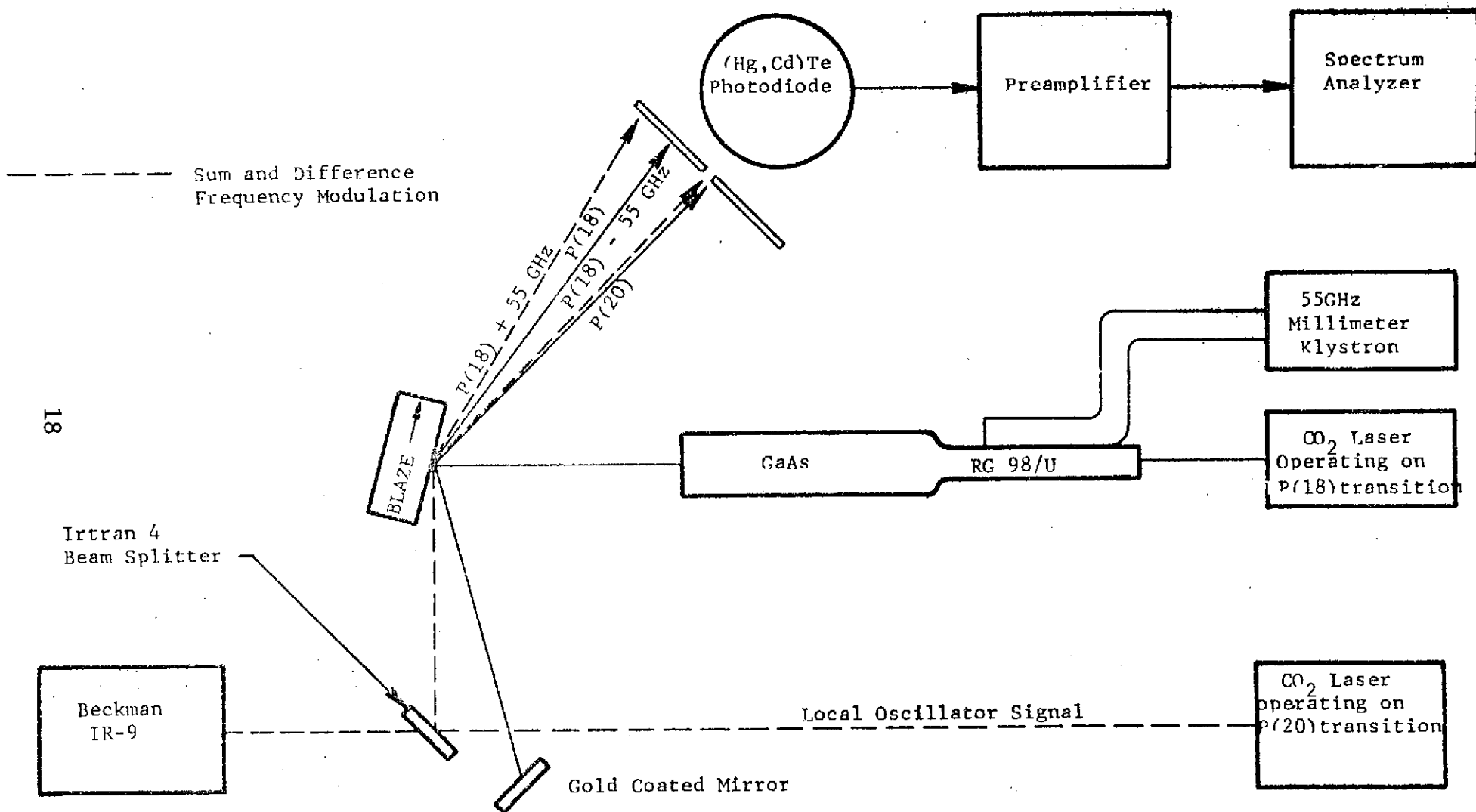


Figure 6 DIAGRAM OF THE KLYSTRON MODULATED CO<sub>2</sub> LASER HETERODYNE SYSTEM

of a single frequency CW CO<sub>2</sub> laser operating on a P branch transition and the millimeter wave signal from a 55 GHz klystron. The sum or difference frequency is detected in a heterodyne receiver with the local oscillator, a CO<sub>2</sub> laser operating on another P-branch laser line. Coherent signals over the 5 GHz tuning range of the klystron are possible.

The preamplifier used was composed of three cascaded Avantek model UA-402. The gain and noise figure is shown in Figure 7.



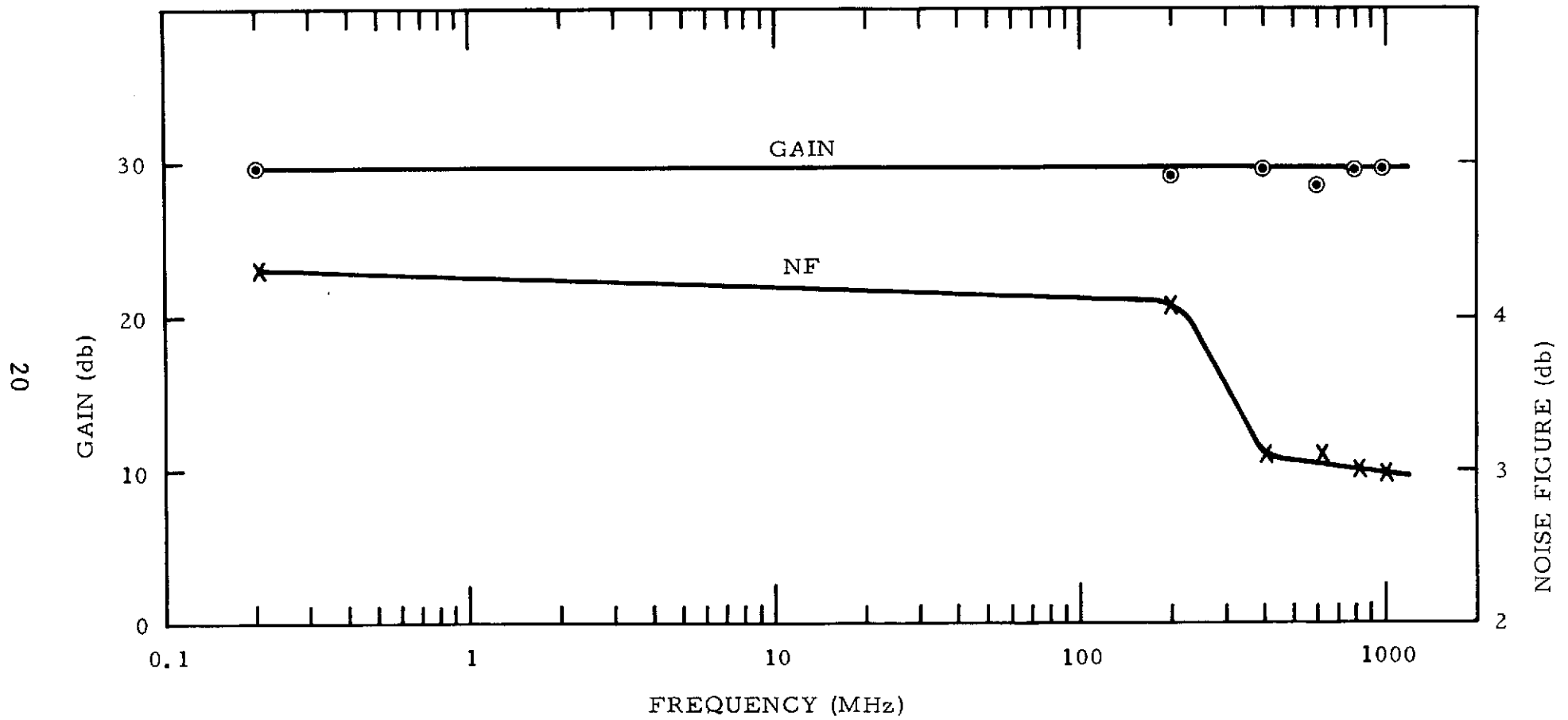


Figure 7 AVANTEK UAA-718B

## SECTION 2

### (Hg,Cd)Te PHOTOVOLTAIC DETECTOR

#### 2.1 JUNCTION FORMATION

Either n on p, or p on n junctions can be formed by diffusion in (Hg,Cd)Te. In the former case, p-type material is heated in a closed quartz ampule containing excess Hg. The latter process is achieved by depositing gold on the n-type material and heating in a controlled environment; either in an open system with a flowing atmosphere of nitrogen and hydrogen or in a sealed quartz tube.

For the Hg diffused diodes, an analytic correlation between time and junction depth could not be made beyond the fact that increasing time usually increased junction distance. The amount of increase was erratic. Table 2.1 summarizes Hg diffusion data including experimental conditions used. As the data indicates, the results were completely substrate dependent. An analytic investigation into the properties of Hg diffusion into (Hg,Cd)Te was beyond the scope of the program.

#### 2.2 DIODE FABRICATION

Following the diffusion process several different techniques for forming diodes were investigated. The results for diodes formed from Ingot 95 V indicate that high quality devices can be made in (Hg,Cd)Te. The major difficulty uncovered by this program is that the diode junction is usually too obscured by surface leakage. All of the reasons are not known, but the fact that diodes whose surfaces are not protected by some sort of passivation are characterized by low (100 ohm) surface shunts. Since surface inversion is known to occur in p-type (Hg,Cd)Te, it probably is a major source of leakage current. This effect is shown in Figure 8 where spot scan data shows response outside the active area suggestive of an inverted surface. Its effect can be overcome by making the surface  $P^+$  with gold diffusion. Recently, evidence has been reported that a ZnS coating on the surface prevents inversion. Diodes fabricated on recent programs indicate that good junctions can be made by forming mesa diodes and using ZnS passivation.

TABLE 2.1

SUMMARY OF Hg DIFFUSION DATA ON (Hg,Cd)Te FOR VARIOUS EXPERIMENTAL CONDITIONS

	Sample Temp.	Hg. Temp.	Time (min.)	Post-Treatment	$x_j, \mu$	$\rho_s$ , ohms/ $\square$ (77K)	C/A, $\Omega$ , 7; pf/cm <sup>2</sup>
20769 S125 B-3	315°C 299	330°C 305	15 60	Quench Quench	15-35	10	1.2 x 10 <sup>5</sup>
C-5	315 299	330 305	15 60	Q & E Q			3.5 x 10 <sup>4</sup>
C-6	325	350	60	Q	130		1.2 x 10 <sup>4</sup>
S126 C-1	300	300	60	Q			
C-2	300	300	60	Q			1.2 x 10 <sup>4</sup>
S122 J	275	157	30	Q	7.5		
F	287	230	30	Q		6.3	
60470 S117 G	275	157	30	Q	Did Not Convert		
H	287	230	30	Q	Did Not Convert		
20769 S122 K	275	157	240	Q			
60470 S117 A	275	157	240	Q	Did Not Convert		
60470 S144 A	275	157	240	Q	Did Not Convert		
20769 S164 C-2	300 300	305 290	30 120	* SC**	117	.47	
20769 S164 C-3	300 300	305 290	30 120	* Q	130	.45	
20769 S123 B-2	300	305	30	Q	66	2.3	
20769 S124 C-1	300	300	60	Q	38		
C-2	300	300	60				

\*\*Slow Cool

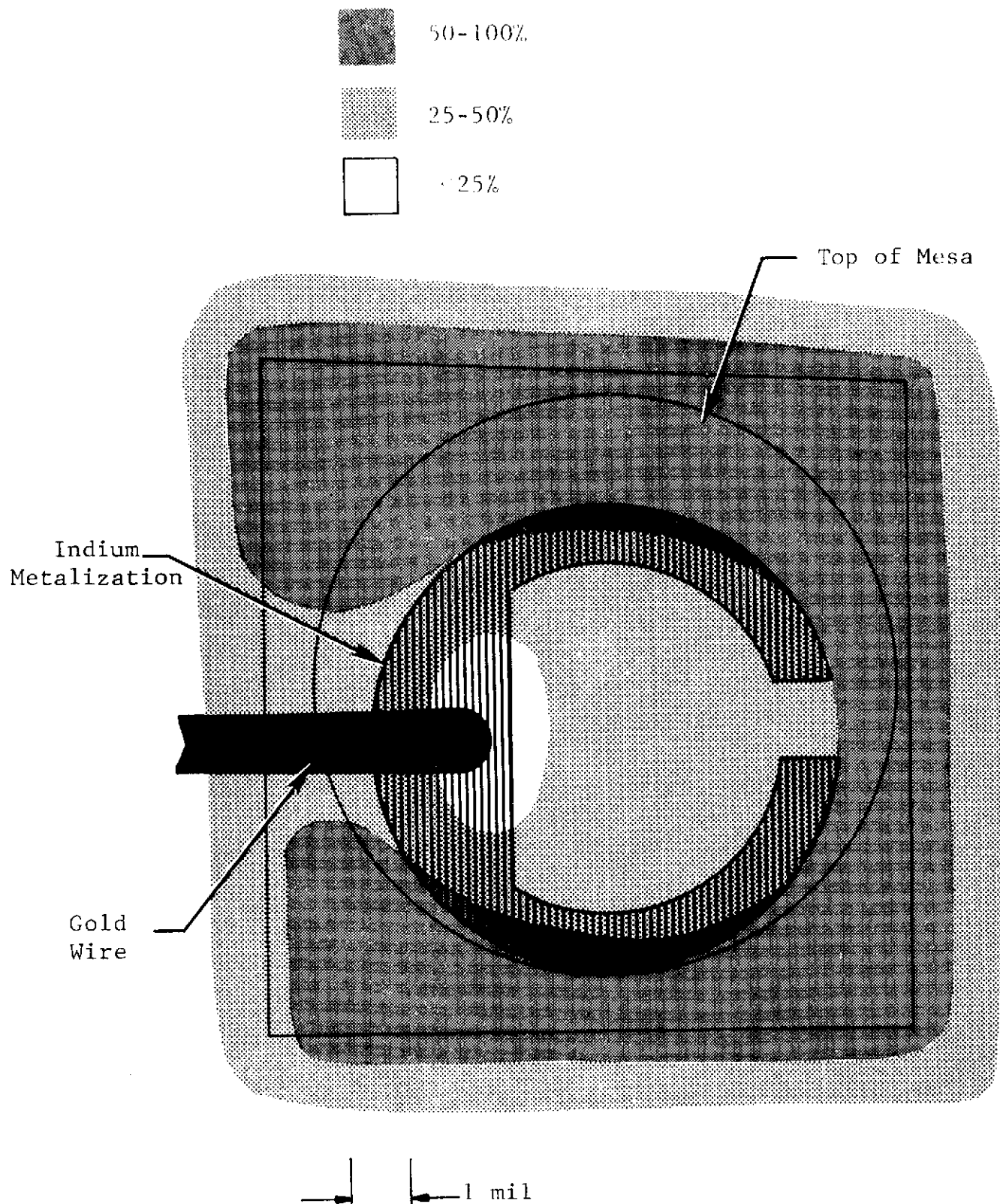


Figure 8 RELATIVE RESPONSIVITY CONTOUR OF AN INITIAL (Hg,Cd)Te PHOTODIODE (Spot Diameter ~2.4 mils)

## 2.3 JUNCTION PROPERTIES FOR Hg DIFFUSED DIODES

### 2.3.1 Temperature Dependence of Reverse Saturation Characteristic

Diodes made from 95 V exhibited good reverse characteristics as shown in Figures 9 and 10. The reverse current almost shows hard saturation indicating that the surface shunt is quite large ( $\sim 10^4$  from the slope of the line). Quite visible is the "knee" in the curve at  $V \sim 4kT$  predicted by equation 22. At this point the current corresponds approximately to the saturation current. The slope of the temperature dependence for  $J_s$  shown in equation 23 corresponds closer to  $n_i$  than  $n_i^2$ , indicating that G-R mechanisms dominate the saturation current. However,  $J_s$  may have a weaker temperature dependence than  $n_i^2$  and still be diffusion limited. If on the p side of the diode Shockly Read recombination is important,  $\tau_e$  can have an exponential temperature dependence. This occurs if the Fermi level lies above the trap level at some elevated temperature. When this happens, the center will be nearly full of electrons and the recombination time (lifetime) very long. As the temperature is lowered, the Fermi level sweeps through the center and it becomes depopulated, and the probability of electron capture becomes very large (small lifetime). Analytically, from S-R theory:

$$\tau_n = \frac{1}{N + \left[ 1 + \frac{n}{p} \frac{\tau_p}{\tau_n} \right] \left[ \frac{r_c(1-f)}{1 + \frac{1-f}{f} \left( \frac{r_c n}{r_{vp}} \right)} \right]^{-1}} \quad (32)$$

For p-type material:

$$\tau_n \sim \frac{1}{N_t r_c (1 - f)} \quad (33)$$

Thus, as  $f$  sweeps from  $\sim 1$ , full occupation, to  $f \sim 0$  (empty),  $\tau_n$  changes exponentially from large value to a small constant value. The temperature dependence of the saturation current due to electron injection therefore need not depend on temperature as  $n_i^2$ , but could easily show a weaker dependence.

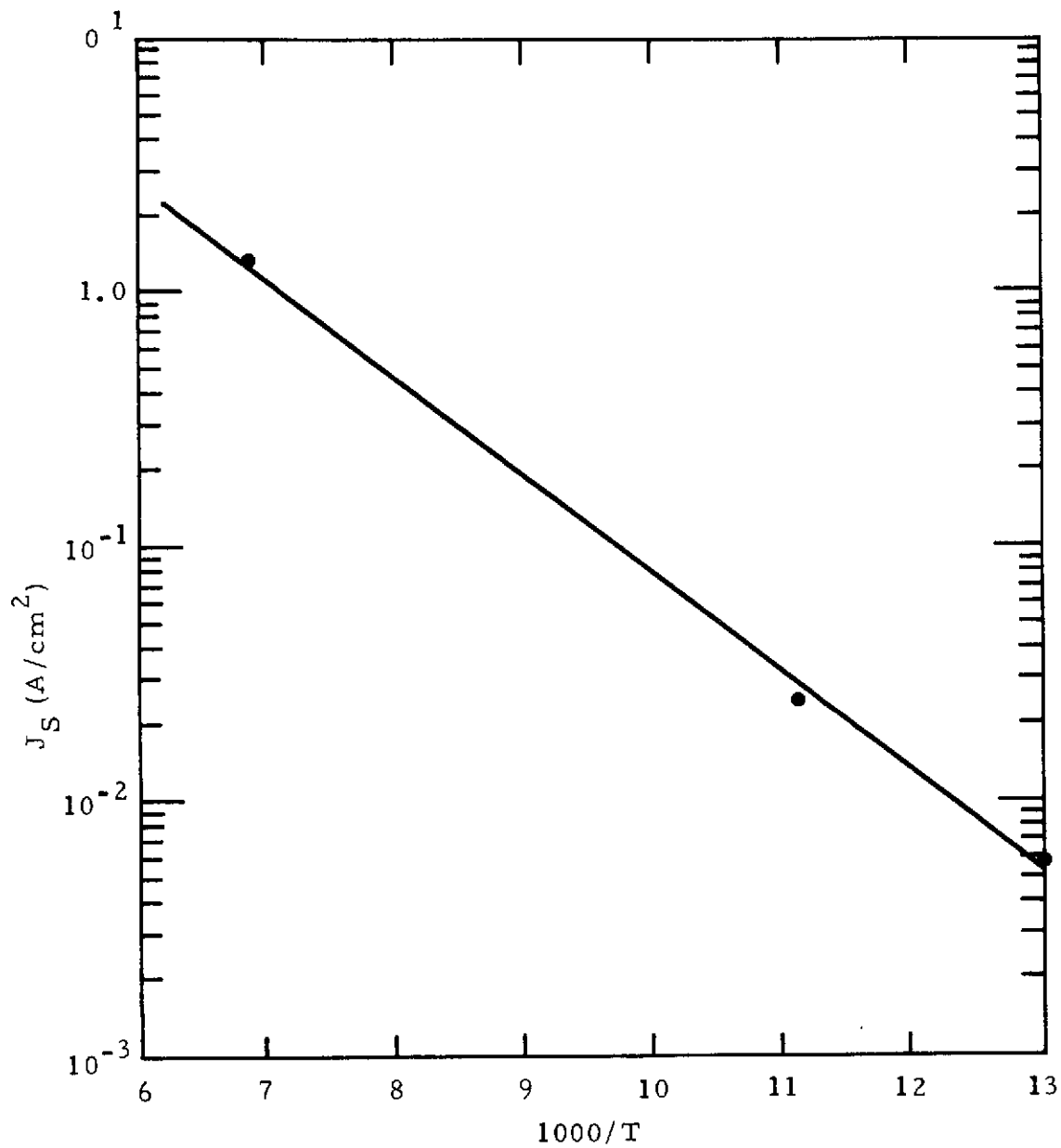
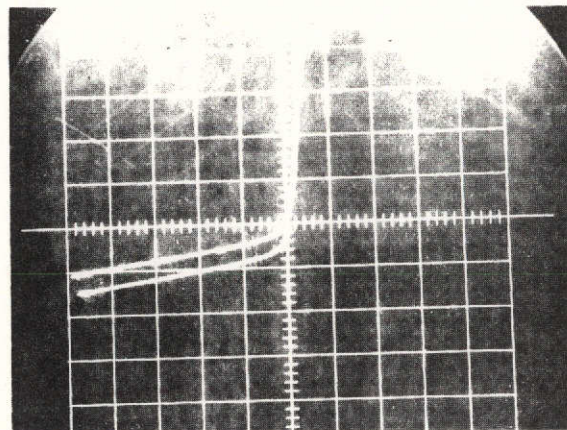
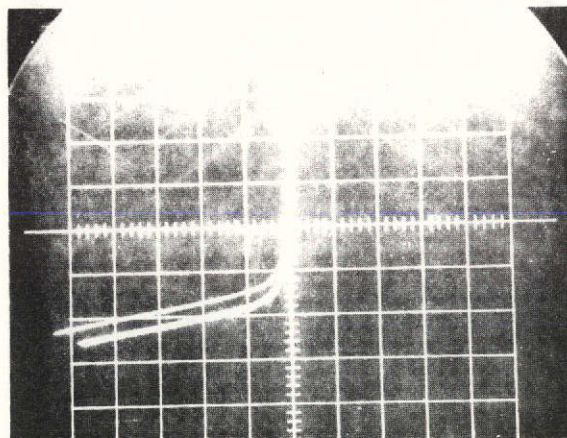


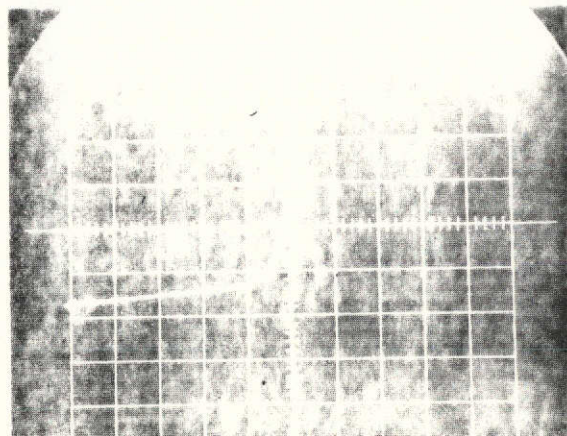
Figure 9 TYPICAL CHARACTERISTIC OF REVERSE SATURATION CURRENT VS TEMPERATURE FOR Hg DIFFUSED (Hg,Cd)Te 10.6  $\mu\text{m}$  PHOTODIODES



77°K  
20  $\mu\text{a}/\text{cm}$   
0.05  $\text{v}/\text{cm}$



90°K  
20  $\mu\text{a}/\text{cm}$   
0.05  $\text{v}/\text{cm}$



146°K  
1  $\text{ma}/\text{cm}$   
0.05  $\text{v}/\text{cm}$

Figure 10 CURRENT-VOLTAGE CHARACTERISTICS OF A (Hg,Cd)Te PHOTO-DIODE ( $\lambda_p = 10.8 \mu\text{m}$  at 77 °K) AT SEVERAL TEMPERATURES WITH AND WITHOUT 300 °K BACKGROUND RADIATION. DIODE AREA,  $1 \times 10^{-3} \text{cm}^2$  (15 mil DIAMETER)

The same argument can be applied to the n side of the material so that both components could show a temperature dependence weaker than  $n_i^2$ . The forward characteristic also depends on whether diffusion or G-R dominate, i.e.

$$J_F \sim e^{-q V/n kT} \quad (34)$$

where  $n = 1$  for the former case, and  $n = 2$  for the latter. The experimental variation falls closer to  $n = 2$ , but does not rule out  $n = 1$  altogether.

### 2.3.2 Comparison of Saturation Current with Theoretical Estimate

For sample 95 V,  $J_s = 6 \times 10^{-3} \text{ A/cm}^2$ , and assuming:

$$\begin{aligned} N_D &= 10^{15} \text{ cm}^{-3} && \text{Estimated} \\ N_A &= 10^{17} \text{ cm}^{-3} && \text{From Hall Data} \\ \mu &= 5 \times 10^2 \text{ cm}^2/\text{volt sec} \\ \mu_e &= 5 \times 10^4 \text{ cm}^2/\text{volt sec} \\ \tau_H &= 10^7 && \text{From Photoconductivity in n-type Material} \\ \tau_e &= 10^{-9} \text{ sec} \\ n_i &= 8 \times 10^{13} && x = 0.2 \end{aligned}$$

Equation 23 yields:

$$J_S = qn_i^2 \left[ \frac{L_p}{N_D \tau_p} + \frac{L_n}{n_a \tau_n} \right] = 5.7 \times 10^{-3} \text{ A/cm}^2$$

An important parameter which determines a diode's ultimate performance is the  $R_J(o)A$  product. This value is given by:

$$R_J(o)A = \frac{kT/8}{J_S} = 1.1 \text{ } \Omega \text{ cm}^2 \text{ at } 77 \text{ } ^\circ\text{K}$$



This predicts a value of Johnson noise limited  $D^*$  of:

$$D_J^* = \eta/h\nu \sqrt{\frac{R_J(o)A}{4kT}} \quad \text{Zero Bias}$$

$$= \eta/h\nu \sqrt{\frac{R_J(o)A}{2kT}} \quad \text{Reverse Bias}$$

For  $\eta = 0.5$ ,  $h\nu = 0.115$  eV,  $4kT = 16 \times 10^{-21}$  joule at 77 °K

$$D^* = 3.45 \times 10^{10} \quad \text{Zero Bias}$$

$$= 4.9 \times 10^{10} \quad \text{Reverse Bias}$$

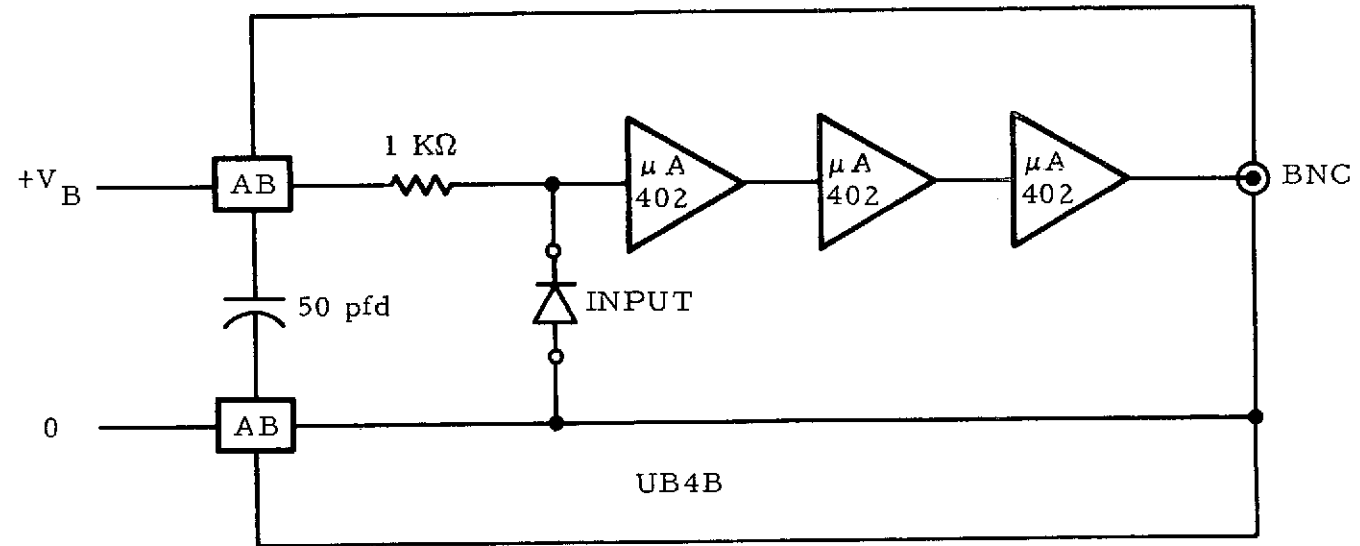
### 2.3.3 Frequency Response Measurement

Frequency response measurements were made on the two units delivered as a contract requirement. The measurements were made at Martin Marietta Corporation in collaboration with Dr. V. Corcoran. The measurement technique has been described in Section 1.2.

The amplifier used in the measurement was Avantek Model UAA-718B, which consisted of a sequence of three modules: UA-401, UA-402, and UA-403 in a UB4B pack. The first stage was modified to include a bias circuit as shown in Figure 11. The detector and amplifier assembly are shown in Figure 12. The gain was 29 dB from 0.2 MHz to 1 GHz. The noise figure was less than 4.1 dB from 0.2 MHz to 1 GHz.

The diodes were reverse biased at 0.2 volt. The data is summarized in Figures 13 and 14. The absolute value of the signal power was not known. A double time constant is apparent in both devices. This is due to different diffusion transit times in the n and p layers of the diode. At low frequencies the signal from the n-side dominates. This layer has a -3 dB point at 19 MHz, indicating a hole transit time of 8.4 ns. The second plateau has a -3 dB point at 110 MHz, indicating a response time of 1.45 ns.

The package transfer function expression gives two terms which may limit the bandwidth. First, the capacitance resistance product gives a response time,



VB 0 TO +4 VOLTS  
AB -

DETECTOR BIAS  
RF FEED-THRU

Figure 11 DETECTOR BIAS RF FEED-THRU

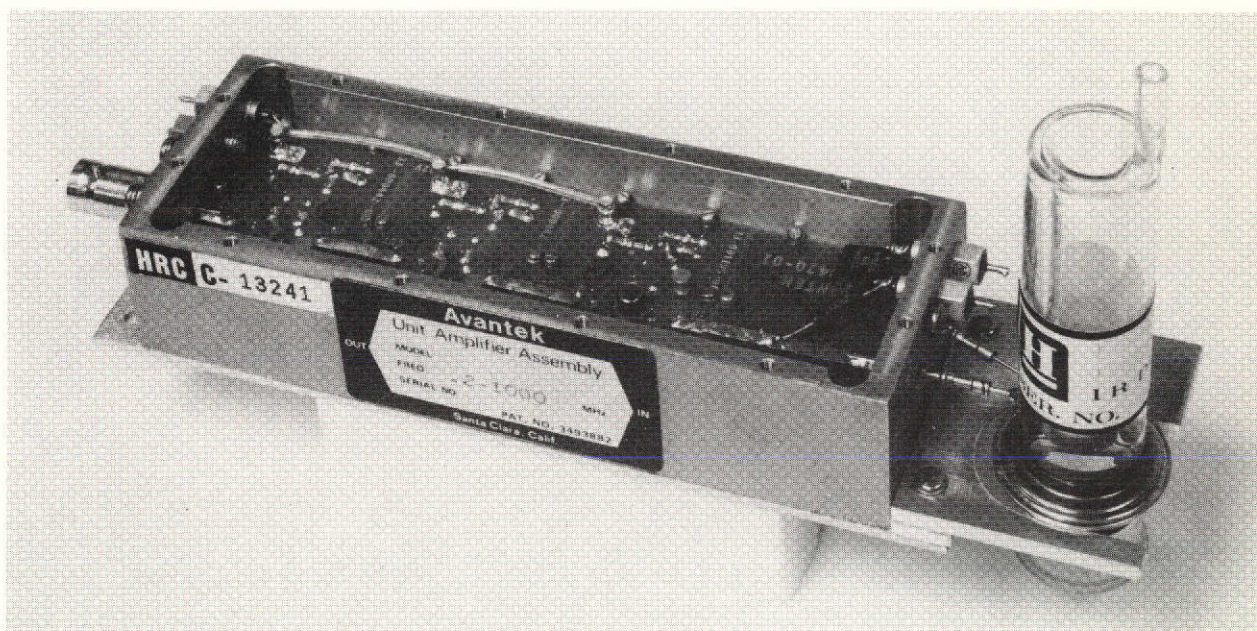


Figure 12 HIGH SPEED (Hg,Cd)Te DETECTOR PREAMPLIFIER  
MODULE FOR 10.6 MICRON RADIATION

PART NUMBER LK132A1  
SERIAL NUMBER W2

- FREQUENCY VS NOISE -  
AND  
SIGNAL

TEST REPORT 3338  
PAGE 4 OF 8

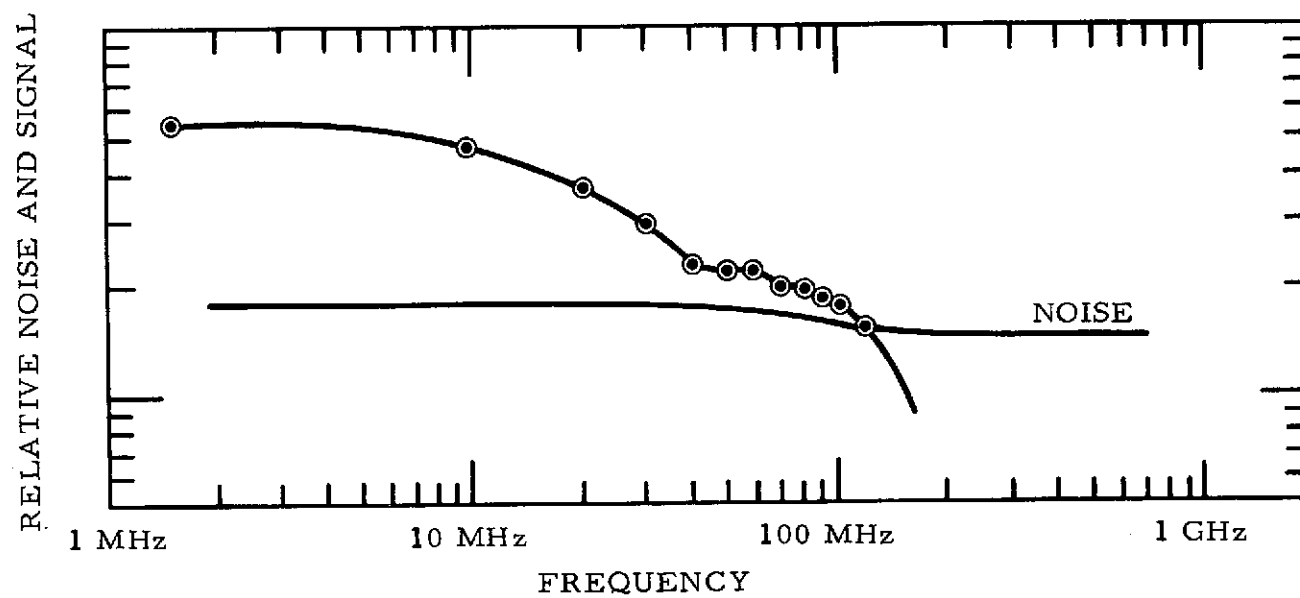


Figure 13 FREQUENCY VS NOISE AND SIGNAL

PART NUMBER LK132A1  
SERIAL NUMBER W1

- FREQUENCY VS NOISE -  
AND  
SIGNAL

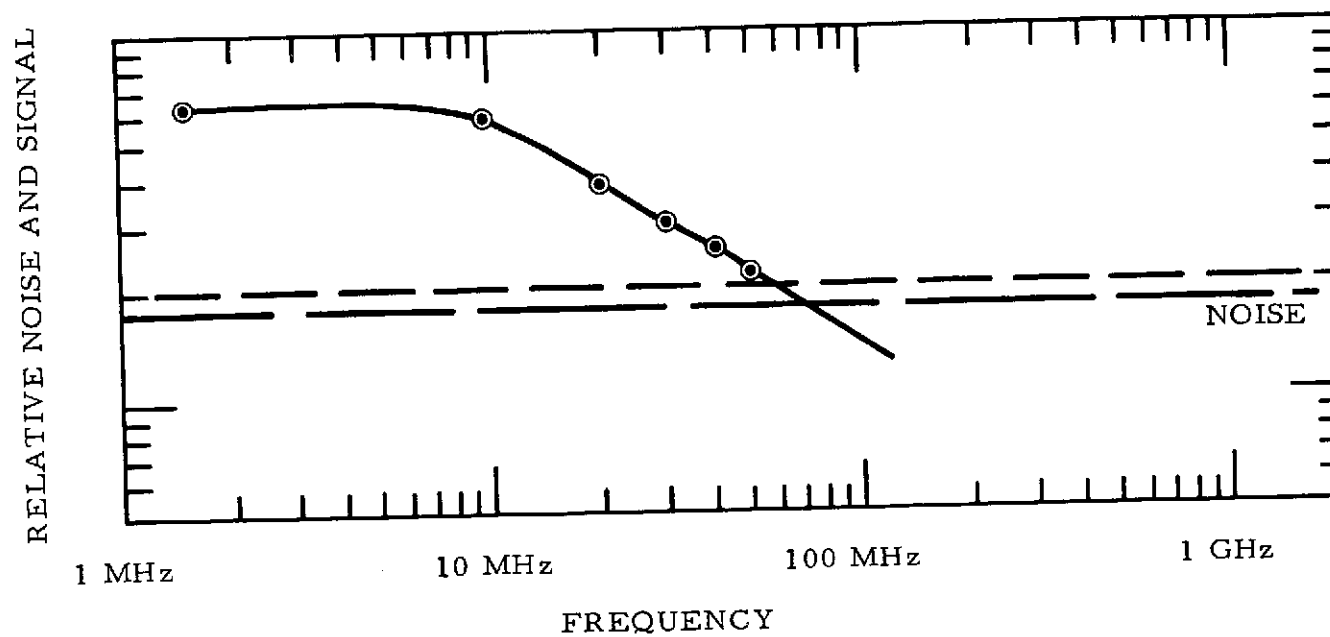


Figure 14 FREQUENCY VS NOISE AND SIGNAL

$$\begin{aligned}\tau &= R_L C_D \\ &= 50 \, \Omega \times 20 \, \text{pfd} \\ &= .1 \, \text{ns} ,\end{aligned}$$

which would give a bandwidth of 1.6 GHz. Second, the package inductance gives a response time,

$$\tau = L/R_J ,$$

where L is inductance in henries. For the radial lead packages used, the inductance was of the order of  $6 \times 10^{-8}$  henry.

The inductance of the package generally would not be a problem for an ideal diode with a high junction resistance ( $R_J$ ). In the units delivered, however,  $R_J$  was 40 ohms.

Therefore,

$$\tau_{L/R} = \frac{6 \times 10^{-8}}{40} = 1.5 \times 10^{-9} \, \text{s} .$$

This corresponds to a bandwidth limit of 106 MHz and agrees with the measured response. A solution to this problem would be to use a coaxial 50-ohm transmission line for the 50-ohm devices. A twin line transmission line could still be used for high resistance junctions. In this case, the lower capacitance of the twin-line can be exploited successfully.

The inductance capacitance product of a transmission line is a constant

$$LC = \mu_0 \epsilon_0 .$$

For a twin line transmission line with 0.065  $\mu\text{H}$  inductance the capacitance would be 0.04 pfd, assuming a vacuum as dielectric.

The coaxial transmission line has a much higher capacitance, and a correspondingly low inductance. A coaxial line with 10 pfd would have an inductance of  $1.1 \times 10^{-10}$  henries. And a 40-ohm detector would not be limited by inductance at frequencies below 58 GHz.

In this case the limit would be the capacitance and amplifier impedance or the device transit time.

### SECTION 3

#### CONCLUSIONS AND RECOMMENDATIONS

The units delivered on this program did not meet the program design goal of 800 MHz bandwidth and 20% quantum efficiency. The units delivered had a 110 MHz 3 dB rolloff frequency which was attributed to the inductive limitations of the package. The package was designed for 400-ohm diode resistances; however, at the time of delivery only 50-ohm devices were available. We feel the device is capable of frequencies in excess of 400 MHz if mounted in a 50-ohm coaxial line package.

It has been concluded that the 800 MHz 20% quantum efficiency is the  $\eta \cdot f^*$  limit of p-type (Hg,Cd)Te with minority carrier mobility of  $10^5 \text{ cm}^2/\text{V-S}$  and no antireflection coating. Improvement in  $f^*$  to 2 GHz is possible but it would mean a sacrifice in quantum efficiency ( $\eta^*$ ) considerably below 20% at that frequency.

If this type of performance is necessary for ultimate systems, we recommend a basic research program on p-type material growth and minority carrier property characterization before any further device fabrication. The goal of this effort would be the feasibility of finding material with higher electron mobility than  $5 \times 10^5 \text{ cm}^2/\text{V-S}$ . An alternate approach would also be a materials development effort to produce epitaxial (Hg,Cd)Te with the ultimate goal of producing p-i-n structures.

## GLOSSARY

$\alpha$	Absorption coefficient
$\Delta f$	Bandwidth
$\epsilon_0$	Dielectric constant of air
$\eta$	Quantum efficiency
$\mu_n, \mu_p$	Mobility of electron, hole
$\tau_n, \tau_p$	Electron, hole response times
$\tau_r$	Recombination time within junction
$\omega$	Angular frequency
$d$	Substrate thickness
$f$	Frequency
$f_c$	Cut-off frequency
$i_a$	Amplifier current noise
$\overline{i_B}^2$	Shot noise associated with background
$\overline{i_J}^2$	Johnson noise of diode
$i_n$	Diode noise current
$i_s$	Diode signal current
$\overline{i_S}^2$	Shot noise of diode
$\overline{i_{Sn}}^2$	Thermal noise of shunt
$k$	Boltzmann's constant
$n$	Electron concentration
$n_i$	Intrinsic carrier concentration
$\rho$	Hole concentration



$q$	Electronic charge
$r$	Reflectivity
$r_c$	Transition probability of electron from trap into conduction band
$r_r$	Transition probability of electron from hole into valence band
$t$	Time
$V_a$	Amplifier voltage noise source
$v_{\text{drift}}$	Drift velocity
$X$	Distance
$A$	Open loop gain
$C$	Impurity concentration
$C_j$	Junction capacitance
$D_n$	Diffusion coefficient of electrons
$D_p$	Diffusion coefficient of holes
$K$	Dielectric constant
$L$	Dewar inductance
$L_n$	Diffusion length of electron
$L_p$	Diffusion length of hole
$N_A$	Acceptor concentration
$N_B$	Carrier concentration due to background
$N_D$	Donor concentration
$N_t$	Trap concentration
$Q_B$	Background photon flux

$R_F$	Amplifier feedback impedance
$R_j$	Incremental junction resistance
$R_L$	Amplifier input impedance
$R_O$	Zero bias junction resistance
$R_S$	Diode series resistance
$R_{Sh}$	Diode shunt resistance
$S$	Surface recombination velocity
$T$	Temperature of diode
$V_{Bi}$	Built-in voltage
$W$	Depletion width
$X_j$	Junction depth

## APPENDIX A

### TEST RESULTS ON 10.6 MICRON (Hg,Cd)Te PHOTODIODES

#### A.1 ION IMPLANTED PV-(Hg,Cd)Te ARRAY

Detectors 1 and 2 of PV-(Hg,Cd)Te Array 11171-80-21 were evaluated at AIL. The photodetectors were 0.0095 inch on a side, and were mounted on a single slab.

Detector 1 exhibited an unusual current voltage characteristic (see Figure A.1) which includes:

1. a soft characteristic,
2. photo-induced current in the forward direction,
3. a reverse shunt conductance which was dc and laser bias dependent,
4. a dark current of up to 2.7 mA for  $V_B = -800$  mV, and
5. a laser-induced photocurrent that was bias dependent.

The variation of reverse shunt conductance and photomixer dark current as a function of reverse bias for photodetector 11171-80-21-1 are given in Figure A.2. The large variation of photomixer shunt conductance with LO bias, as well as the induced photocurrent in the forward bias direction, may be due to photoconductive effects in the photodetector or contact problems. It should be noted that these characteristics make this photodiode unusable for most heterodyne receiver applications. An estimate of the 3-dB cutoff frequency for this photodetector at -200 mV reverse bias is 125 MHz with a roll-off of approximately 12 dB/octave. The i-f amplifier impedance and load resistor were 50 ohms and the i-f amplifier had a 30-dB gain. This 12 dB/octave (rather than the usual 6 dB/octave) rolloff may indicate that both RC and transit time effects are limiting the photodetector frequency response.

Detector 2 exhibited a reasonably well-behaved I-V characteristic (see Figure A.3), had a measured 3-dB cutoff frequency near 280 MHz for  $V_B = -300$  mV and  $T_m = 77$  K, a roll-off of 12 dB/octave (RC and transit time limited?), and what appeared to be 1/f noise degradation up to about 10 MHz.

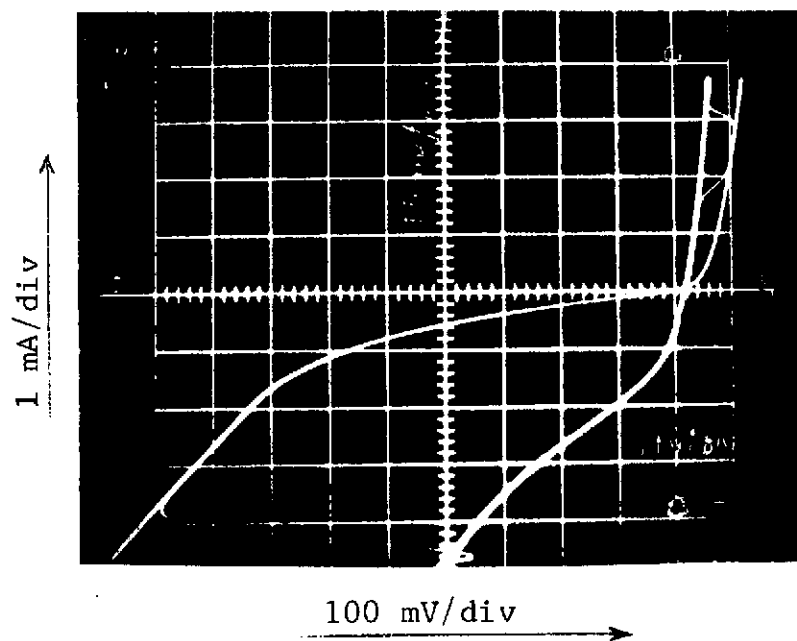


Figure A.1 MEASURED CURRENT-VOLTAGE CHARACTERISTICS OF A PV-(Hg,Cd)Te PHOTOMIXER WITH AND WITHOUT APPLIED LASER LO POWER.

Measurements were carried out on detector 2 to determine the heterodyne receiver sensitivity at an i-f offset frequency of 20 MHz. An NEP of  $3.5 \times 10^{-19}$  W/Hz was measured for  $T_m = 77$  K and  $V_B = -300$  mV, corresponding to an effective photomixer quantum efficiency near 7 percent.

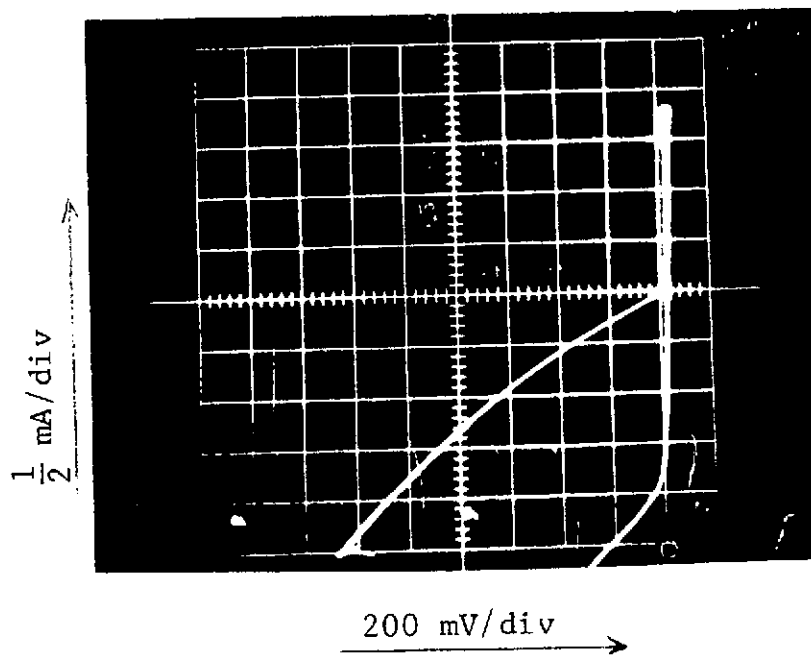


Figure A.2 MEASURED CURRENT-VOLTAGE CHARACTERISTIC OF A PV-(Hg,Cd)Te PHOTOMIXER WITH AND WITHOUT APPLIED LASER POWER

$T_M = 77K$

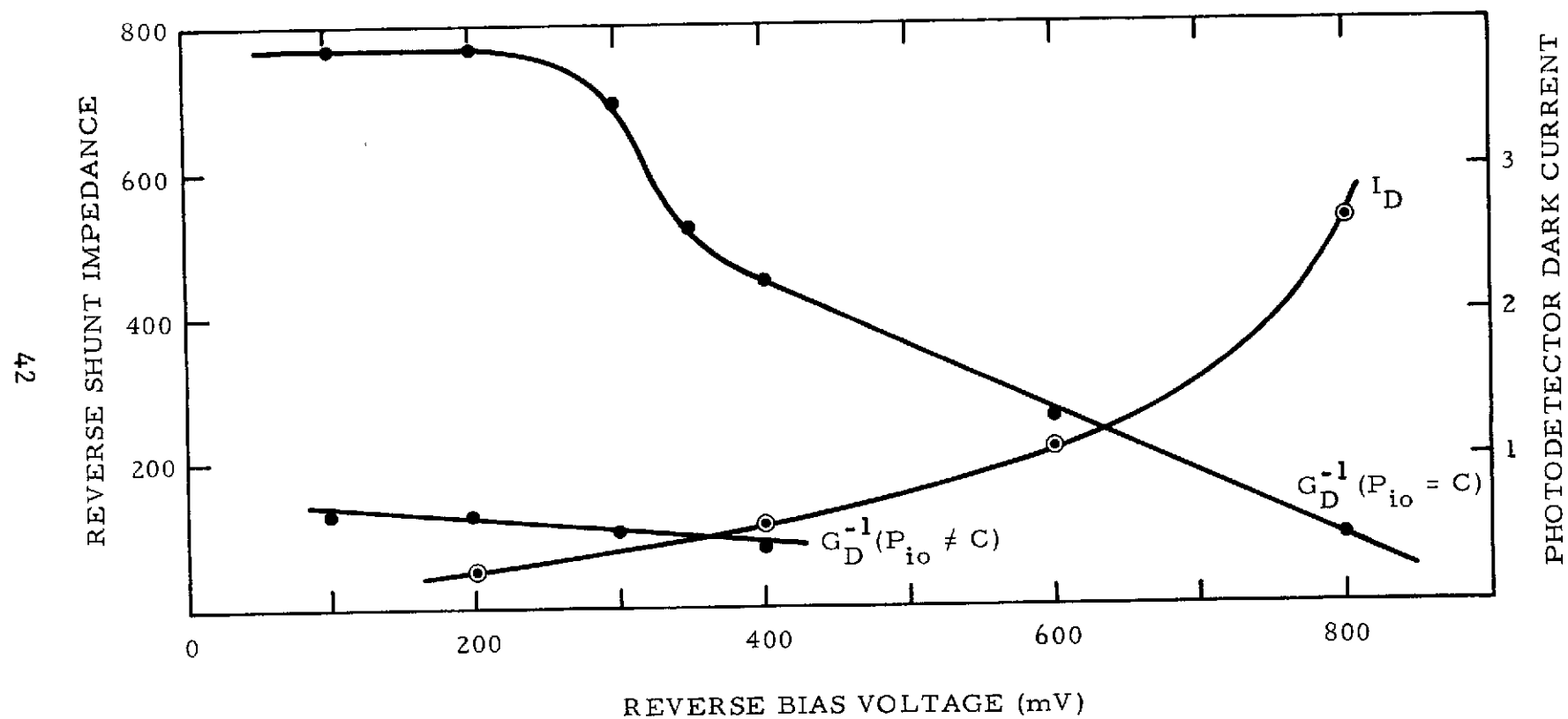


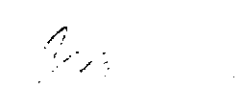
Figure 3.3 MEASURED CHARACTERISTICS OF IV-(Hg,Cd)Te PHOTODETECTOR

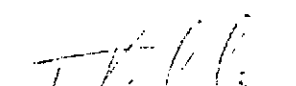
APPENDIX B  
TEST REPORTS FOR DELIVERED UNITS



TEST REPORT NO. 3337  
FOR  
LK132A1 S/N W1 INFRARED DETECTOR  
FOR  
NASA/Goddard Space Flight Center

CUSTOMER P.O. NO.  
NAS5-21197

  
PRODUCT ASSURANCE  
ENGINEER

  
PROJECT ENGINEER

  
PROGRAM MANAGER

Honeywell Inc.  
Radiation Center  
2 Forbes Road  
Lexington, Massachusetts 02173

## TABLE OF CONTENTS

### SECTION

- 1.0 Description of Detector
- 2.0 Test Results
- 3.0 Conditions of Measurement
- 4.0 Detector Readout Circuitry
- 5.0 Handling and Precautions

NOTE: PLEASE READ "HANDLING AND PRECAUTIONS"  
BEFORE USING THIS DETECTOR

(Device) LK132A1 (Series) K1 (S/N) W1

PA 22114-01

Contract No. NAS5-21197

Customer: NASA

1. Description of Detector

HRC Identification Number  
Type of Detector  
Date of Manufacture  
Window Material

95V 115  
Photovoltaic  
November 1972  
Irtran II

Element:

Area

$5.07 \times 10^{-4} \text{ cm}^2$

Liquid Nitrogen Hold Time

> 40 minutes

2. Test Performance Data

Resistance at 77°K  
Detector Time Constant

38 ohms  
 $8 \times 10^{-9}$  sec.

Maximum Bias (not to be  
exceeded)  
Spectral Response Peak

4 ma  
10.0 microns

$D^*_\lambda$  (10, 10KHz, 1)

$1.6 \times 10^{10}$

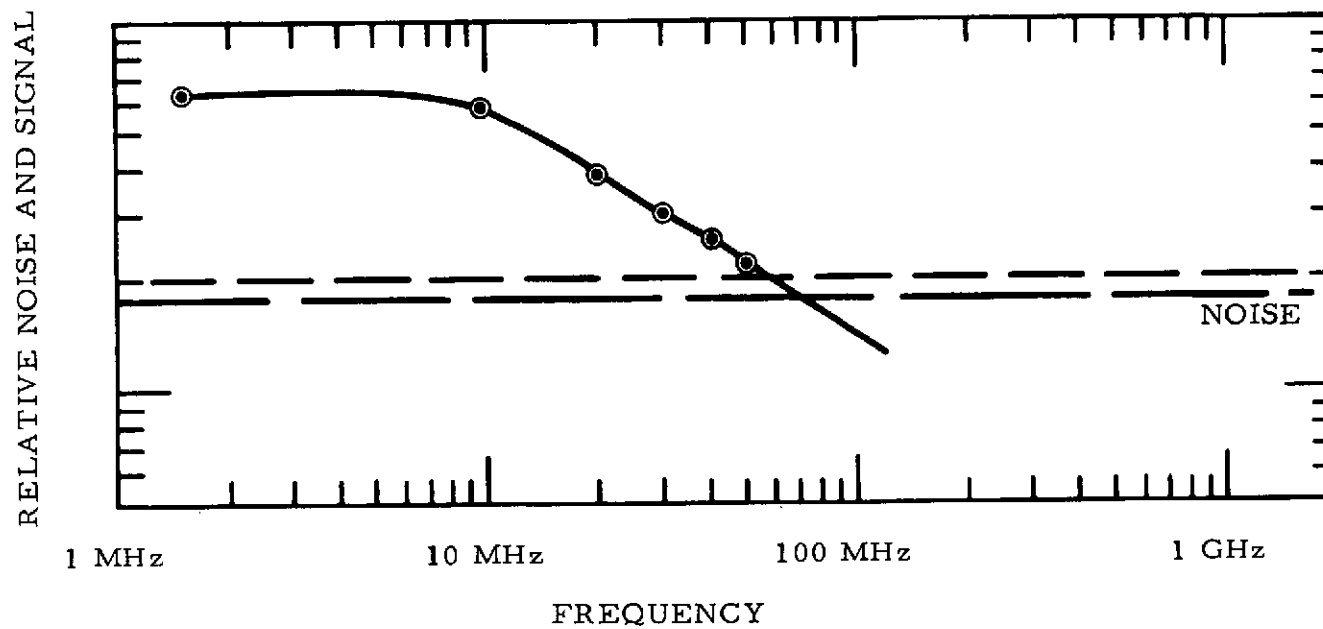
$D^*_p$  (10, , 10KHz, 1)

$2.2 \times 10^{10}$

PART NUMBER LK132A1  
SERIAL NUMBER W1

- FREQUENCY VS NOISE -  
AND  
SIGNAL

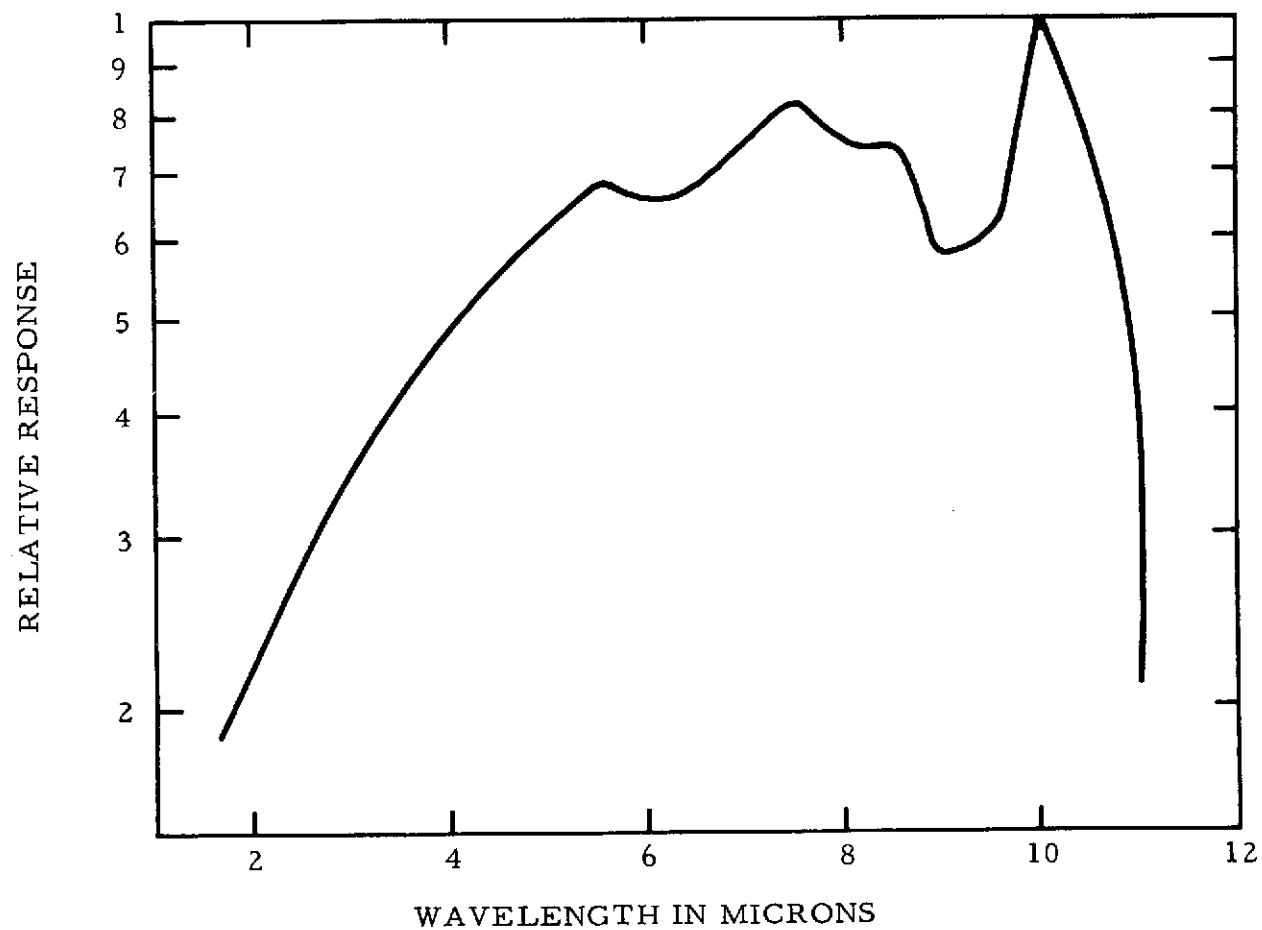
TEST REPORT 3337  
PAGE 4 OF 8



PART NUMBER LK132A1  
SERIAL NUMBER W1

RELATIVE SPECTRAL RESPONSE

TEST REPORT 3337  
PAGE 5 OF 8



# CONDITIONS OF MEASUREMENT

3.0

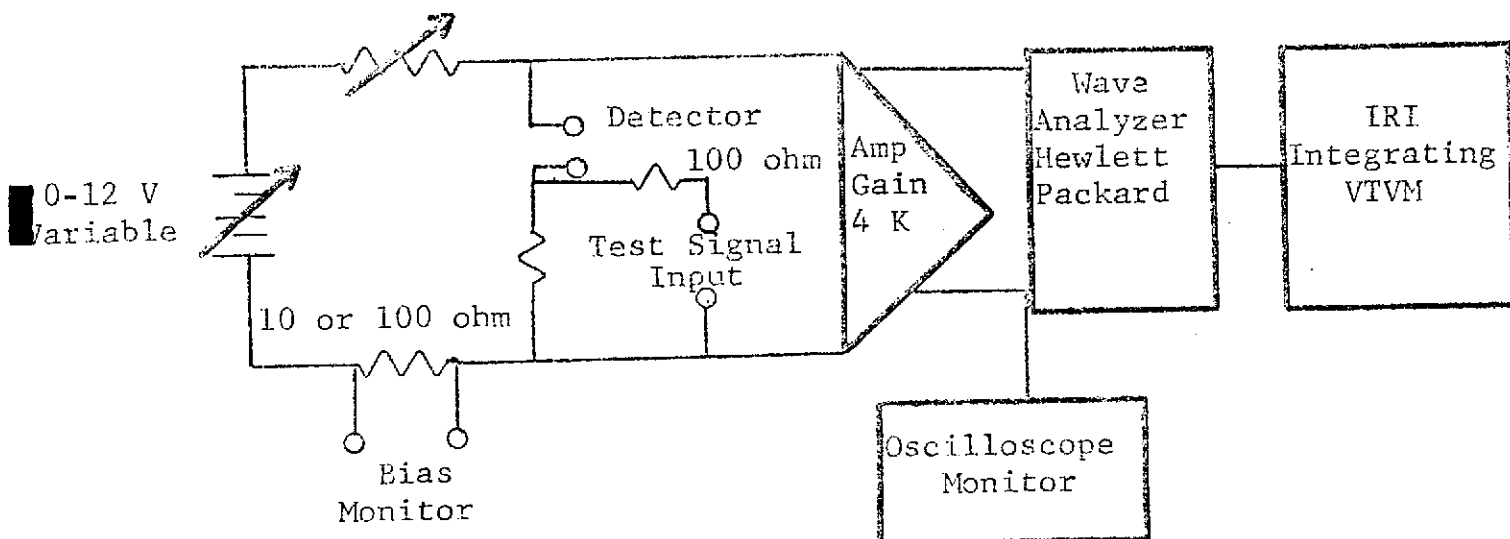
Detector Temperature	77° K
Chopping Frequency	10,000
Detector Area ( $A_D$ )	See Page 3
Orifice Diameter ( $d_B$ )	0.050 inch
Blackbody Temperature ( $T_B$ )	500° K
Background Temperature ( $T_C$ )	300° K
Emissivity	
Blackbody ( $\epsilon_B$ )	1.0
Chopper ( $\epsilon_C$ )	1.0
Noise Bandwidth ( $\Delta f$ )	6 Hz
Chopper RMS Factor ( $K_1$ )	0.35
Detector to Orifice Distance (D)	15 cm
Stefan-Boltzman Constant ( $K_2$ )	$5.67 \times 10^{-12}$
RMS Noise Correction ( $K_3$ )	1.12
Amplifier Gain (same for signal & noise)	100
D* Formula:	

$$D^*_{BB} = \frac{4D^2 (\Delta f)^{1/2}}{K_1 K_2 K_3 d_B^2 \sqrt{A_D} (\epsilon_B T_B^4 - \epsilon_C T_C^4)} \times \frac{S}{N}$$

## DETECTOR READOUT CIRCUITRY

4.0

Variable Load  
100-11 K



## 5.0 HANDLING AND PRECAUTIONS FOR HRC PRECISION INFRARED DETECTORS

This precision infrared detector was built in the laboratories of the Honeywell Radiation Center with the utmost care, using some of the most modern technology. However, as with any precision piece of equipment, there are tolerance limitations to which it can be subjected physically, thermally, and electrically.

### Operating Temperature

The detector is designed to operate at the approximate temperatures noted on page 6

### Window and Housing

Parts may crack or break if subjected to high impact. Always transport the detector in the container in which it was shipped.

### Detector Element Burnout

The detector element dissipates only milliwatts of power, therefore, do not over bias it.

- A. Caution: If a lead from the detector breaks contact with the bias circuit:
  - 1. Turn off bias and amplifier power source.
  - 2. Discharge coupling capacitor by shorting test leads.
  - 3. Re-connect detector element to bias supply.
  - 4. Turn bias power on again.
- B. When the detector is connected to any power source, there must be no voltage differential between the contacts until after the circuit is complete.
- C. Do not use any amplifier circuit that may generate current surges in the detector.

- D. The detector should be operated only in a cooled condition. If the cooling unit may malfunction without operator's knowledge, Honeywell suggests that a current voltage limiter be installed in the bias circuit to prevent burnout when the detector element warms.

Normally, meters used to measure resistance have a 1.5 volt battery. The current generated by the battery is sufficient to burnout the detector. Therefore, if resistance must be measured, observe the following:

- A. Use Wheatstone bridge with an external battery to produce a current/voltage level compatible with Honeywell's test results.
- B. When the detector is in an operating circuit or system, use a VTVM with selector switch set to VOLTAGE. Read voltage drop across detector and compute resistance by Ohm's Law. Be cautious of power ground loops between the VTVM and detector circuitry. Connect common ground first, then connect VTVM to high side of detector. If VTVM is of a high impedance, use a series limiting resistance in VTVM lead. Resistance values up to 1% of VTVM input impedance will cause no voltage reading errors.

#### Moisture

Remove all traces of moisture in the dewar well before cooling the detector. This will minimize thermal transfer problems and prevent dewar well breakage caused by the expansion of water when it freezes.



TEST REPORT 3338

FOR

LK132A1 S/N W2 INFRARED DETECTOR

FOR

NASA/Goddard Space Flight Center

CUSTOMER P.O. NO.

NAS 5-21197

  
PRODUCT ASSURANCE  
ENGINEER

  
PROJECT ENGINEER

  
PROGRAM MANAGER

Honeywell Inc.  
Radiation Center  
2 Forbes Road  
Lexington, Massachusetts 02173

## TABLE OF CONTENTS

### SECTION

- 1.0 Description of Detector
- 2.0 Test Results
- 3.0 Conditions of Measurement
- 4.0 Detector Readout Circuitry
- 5.0 Handling and Precautions

NOTE: PLEASE READ "HANDLING AND PRECAUTIONS"  
BEFORE USING THIS DETECTOR

(Device) LK132A1(Series) K1 (S/N) W2EPA 22114-01Contract No. NAS5-21197Customer: NASA1. Description of Detector

HRC Identification Number  
Type of Detector  
Date of Manufacture  
Window Material

95V 115PhotovoltaicNovember 1972Irtran IIElement:

Area

 $5.07 \times 10^{-4} \text{ cm}^2$ 

Liquid Nitrogen Hold Time

30 minutes2. Test Performance Data

Resistance at 77°K  
Detector Time Constant

37 ohms $1.33 \times 10^{-9}$  seconds

Maximum Bias (not to be  
exceeded)

4 ma

Spectral Response Peak

10 micronResponsivity,  $R_\lambda$ .737 A/W

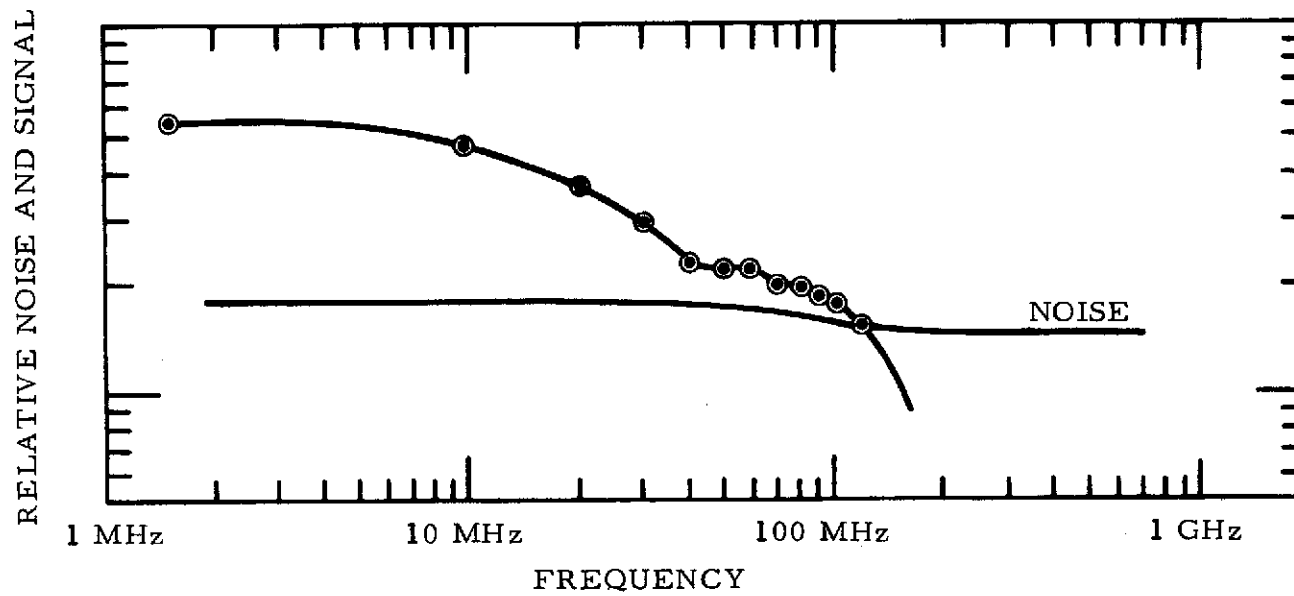
Quantum Efficiency

20%

PART NUMBER LK132A1  
SERIAL NUMBER W2

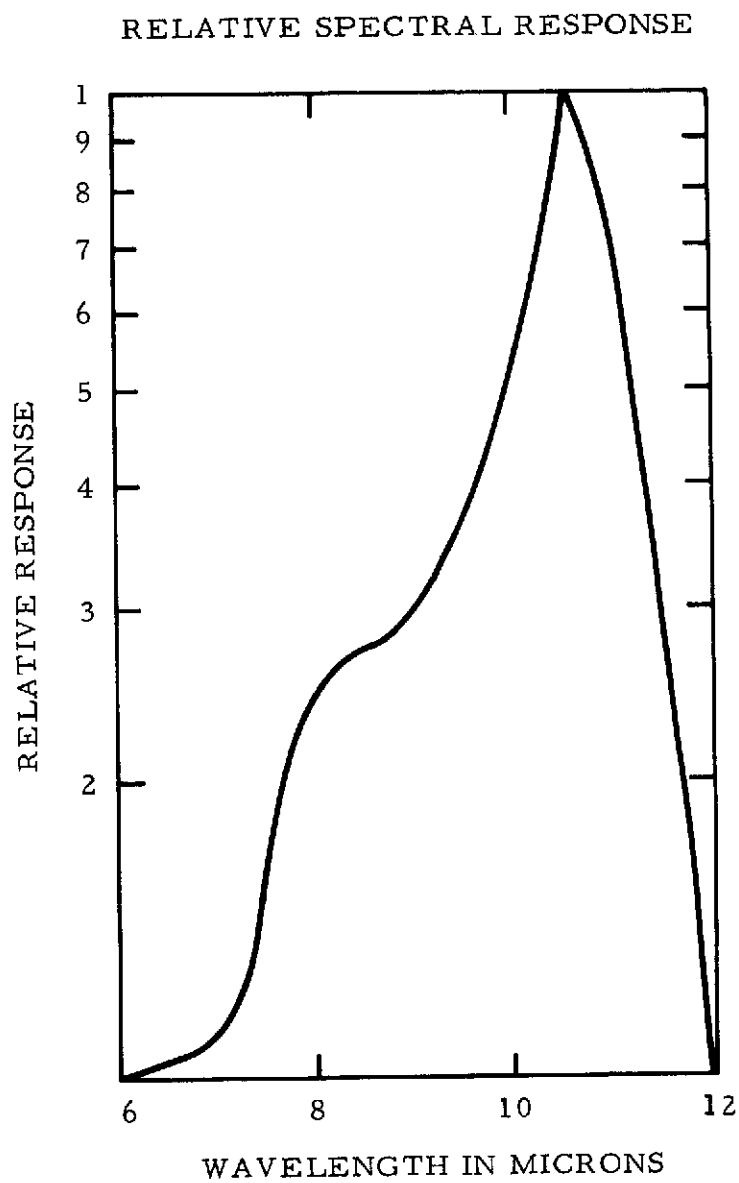
- FREQUENCY VS NOISE -  
AND  
SIGNAL

TEST REPORT 3338  
PAGE 4 OF 8



PART NUMBER LK132A1  
SERIAL NUMBER W2

TEST REPORT 3338  
PAGE 5 OF 8



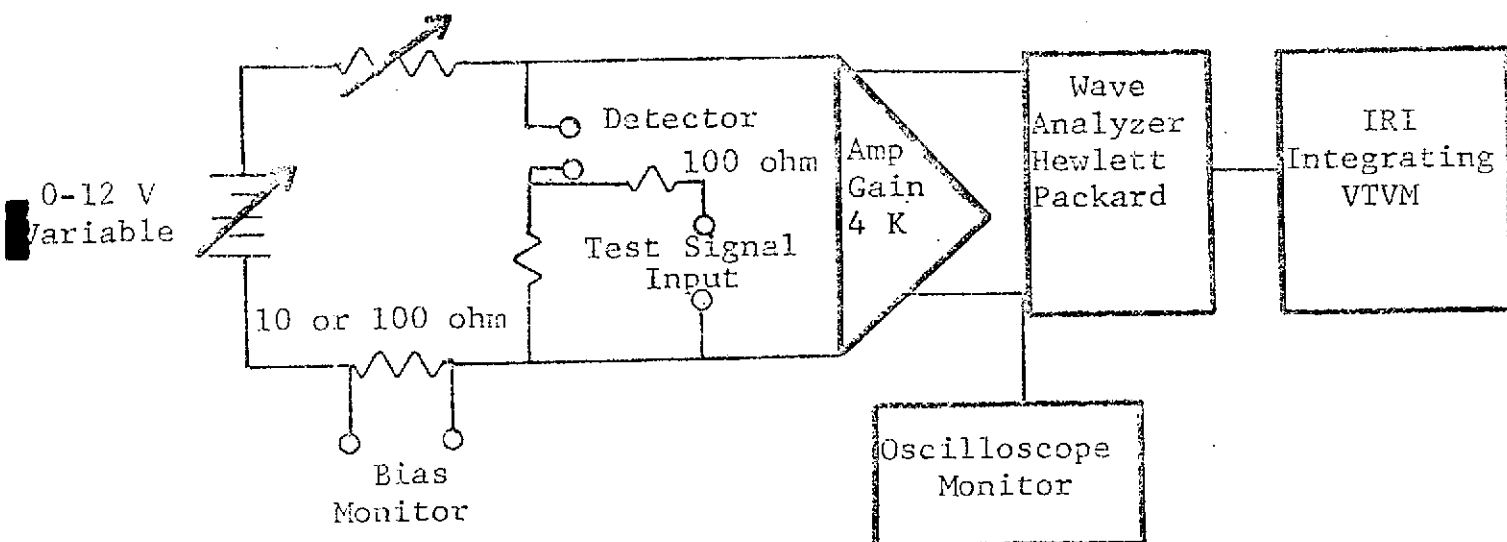
# CONDITIONS OF MEASUREMENT

Detector Temperature	77° K
Chopping Frequency	10,000
Detector Area ( $A_D$ )	See Page 3
Orifice Diameter ( $d_B$ )	0.050 inch
Blackbody Temperature ( $T_B$ )	500° K
Background Temperature ( $T_C$ )	300° K
Emissivity	
Blackbody ( $\epsilon_B$ )	1.0
Chopper ( $\epsilon_C$ )	1.0
Noise Bandwidth ( $\Delta f$ )	6 Hz
Chopper RMS Factor ( $K_1$ )	0.35
Detector to Orifice Distance (D)	15 cm
Stefan-Boltzman Constant ( $K_2$ )	$5.67 \times 10^{-12}$
RMS Noise Correction ( $K_3$ )	1.12
Amplifier Gain (same for signal & noise)	100
D* Formula:	

$$D^*_{BB} = \frac{4D^2 (\Delta f)^{1/2}}{K_1 K_2 K_3 d_B^2 \sqrt{A_D} (\epsilon_B T_B^4 - \epsilon_C T_C^4)} \times \frac{S}{N}$$

## DETECTOR READOUT CIRCUITRY

Variable Load  
100-11 K



## 5.0 HANDLING AND PRECAUTIONS FOR HRC PRECISION INFRARED DETECTORS

This precision infrared detector was built in the laboratories of the Honeywell Radiation Center with the utmost care, using some of the most modern technology. However, as with any precision piece of equipment, there are tolerance limitations to which it can be subjected physically, thermally, and electrically.

### Operating Temperature

The detector is designed to operate at the approximate temperatures noted on page 6

### Window and Housing

Parts may crack or break if subjected to high impact. Always transport the detector in the container in which it was shipped.

### Detector Element Burnout

The detector element dissipates only milliwatts of power, therefore, do not over bias it.

- A. Caution: If a lead from the detector breaks contact with the bias circuit:
  - 1. Turn off bias and amplifier power source.
  - 2. Discharge coupling capacitor by shorting test leads.
  - 3. Re-connect detector element to bias supply.
  - 4. Turn bias power on again.
- B. When the detector is connected to any power source, there must be no voltage differential between the contacts until after the circuit is complete.
- C. Do not use any amplifier circuit that may generate current surges in the detector.

- D. The detector should be operated only in a cooled condition. If the cooling unit may malfunction without operator's knowledge, Honeywell suggests that a current voltage limiter be installed in the bias circuit to prevent burnout when the detector element warms.

Normally, meters used to measure resistance have a 1.5 volt battery. The current generated by the battery is sufficient to burnout the detector. Therefore, if resistance must be measured, observe the following:

- A. Use Wheatstone bridge with an external battery to produce a current/voltage level compatible with Honeywell's test results.
- B. When the detector is in an operating circuit or system, use a VTVM with selector switch set to VOLTAGE. Read voltage drop across detector and compute resistance by Ohm's Law. Be cautious of power ground loops between the VTVM and detector circuitry. Connect common ground first, then connect VTVM to high side of detector. If VTVM is of a high impedance, use a series limiting resistance in VTVM lead. Resistance values up to 1% of VTVM input impedance will cause no voltage reading errors.

#### Moisture

Remove all traces of moisture in the dewar well before cooling the detector. This will minimize thermal transfer problems and prevent dewar well breakage caused by the expansion of water when it freezes.